

Electronic structure and anion ordering in $(\text{TMTSF})_2\text{ClO}_4$ and $(\text{TMTSF})_2\text{NO}_3$: A first-principles study

Pere Alemany,¹ Jean-Paul Pouget,² and Enric Canadell³

¹*Departament de Química Física and Institut de Química Teòrica i Computacional (IQTCUB), Universitat de Barcelona, Martí i Franquès 1, 08028 Barcelona, Spain*

²*Laboratoire de Physique des Solides, Université Paris-Sud, CNRS-UMR 8502, F-91405 Orsay, France*

³*Institut de Ciència de Materials de Barcelona (CSIC), Campus UAB, 08193 Bellaterra, Spain*

(Received 23 December 2013; revised manuscript received 2 April 2014; published 17 April 2014)

A first-principles density functional theory study of the Bechgaard salts $(\text{TMTSF})_2\text{ClO}_4$ and $(\text{TMTSF})_2\text{NO}_3$, with special emphasis on the anion ordering transition, is reported. It is found that the main effect of the anion ordering on the band structure occurs through the deformations induced in the TMTSF layers and not through the Coulomb potential of the anions, as it has been almost invariably assumed. It is shown that the anion ordering in $(\text{TMTSF})_2\text{ClO}_4$ leads to a modulation of the dimerization in successive chains and to a noteworthy polarization of the two partially filled bands around the Fermi level into either the TMTSF A or TMTSF B donors. The calculated anion ordering half gap Δ_{AO} is found to be small but definitely non-nil, ~ 14 meV. The suppression of the SDW instability in the relaxed samples is attributed to the deterioration of the Fermi surface nesting in the anion ordered phase. The possible nodal structure of the superconducting gap is discussed in relation with the newly calculated split Fermi surface. Anion ordering in $(\text{TMTSF})_2\text{NO}_3$ leads to a smaller half gap, 8.9 meV. The anion ordering in this salt leads to a larger charge transfer between the two donors but to a smaller polarization of the two partially filled electron and hole bands. The weak influence of anion ordering into the low-temperature physics of this salt is related to the different periodicity of the anion ordering which leaves the nested parts of the Fermi surface almost unaltered.

DOI: [10.1103/PhysRevB.89.155124](https://doi.org/10.1103/PhysRevB.89.155124)

PACS number(s): 64.70.kt, 71.20.Rv, 71.30.+h, 75.30.Fv

I. INTRODUCTION

The Bechgaard salts $(\text{TMTSF})_2X$ (where TMTSF stands for tetramethyltetraselenafulvalene and $X = \text{PF}_6, \text{ClO}_4, \text{NO}_3, \text{BF}_4$, etc.) have been the focus of vast interest since the discovery of superconductivity under pressure in $(\text{TMTSF})_2\text{PF}_6$ [1]. Their quasi-one-dimensional (Q1D) electronic structure as well as the occurrence of sizable electron-electron interactions leads to a complex phase diagram with several competing ground states [2,3]. As shown in Fig. 1, these salts are built from zigzag chains (i.e., the chains are dimerized) of TMTSF donors along the a direction, which stack into ab layers [4]. The anions reside in the interlayer holes resulting from the zigzag nature of the chains.

The band structure of these salts can be simply understood on the basis of the spread into bands of the highest occupied molecular orbital (HOMO) of the TMTSF donors [5]. These bands are partially emptied because of the presence of the charged anions in the lattice. However, since the anions do not participate in any sizable way on the electronic states near the Fermi level, their role, except for some gross features, has often been ignored. Although many aspects of the physics of these archetypal Q1D systems seem by now reasonably well understood, several important questions still remain unanswered. A key aspect in settling some of these issues relies in clearly understanding the role of anions. Because of their relative structural freedom within the interlayer cavities, they undergo order-disorder transitions which subtly but crucially affect the physical behavior of these salts [6]. These transitions have been known for a long time [7], but their influence on the low-temperature electronic structure is still far from being satisfactorily understood. At least partially, this situation was due to the lack of reliable-enough first-principles electronic

structure calculations which could address this problem at a microscopic level by treating on the same footing both cations and anions. However, there is now a considerable amount of work showing that present-day density functional theory (DFT)-based approaches are reliable enough to explore the fine details of the electronic structure of molecular conductors [8–17]. In particular, the role of anions on several transitions exhibited by these solids (charge ordering, charge density wave formation, etc.) has been considered [15,16,18]. These works have made clear that anions are far from being innocent spectators simply following the instabilities of the donor's sublattice, as frequently assumed: They are indeed essential players in the process. Here we would like to extend this work to two well-known Bechgaard salts which exhibit anion ordering transitions, $(\text{TMTSF})_2\text{ClO}_4$ and $(\text{TMTSF})_2\text{NO}_3$.

$(\text{TMTSF})_2\text{ClO}_4$ is an ambient-pressure superconductor [19] which exhibits an anion ordering transition at 24 K [20,21]. Its ground state depends of the cooling rate in the vicinity of the anion ordering temperature [6,22]. Under very slow cooling, the samples become superconducting at 1.2 K. For faster cooling rates, the anion ordering is less complete and the samples undergo a $2k_F$ spin density wave (SDW) transition due to Fermi surface nesting, as in other Bechgaard salts [2,3] (k_F is the Fermi wave vector in the stack direction of the Q1D band dispersion). The anion ordering doubles the periodicity along b so that the band structure is folded along b^* and the Q1D Fermi surface splits into two pairs of lines. An important question which is an object of controversy is the magnitude of this splitting. Whereas the tight-binding Fermi surface exhibits a very sizable splitting [21], a recent first-principles study [23] suggests that the split Fermi surfaces merge together inside the Brillouin zone. This is a surprising conclusion which certainly needs further consideration.

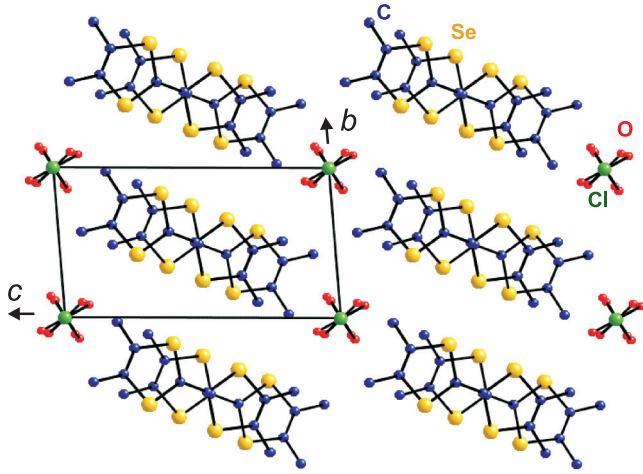


FIG. 1. (Color online) View of the room-temperature crystal structure of $(\text{TMTSF})_2\text{ClO}_4$ along a . For clarity, hydrogen atoms are not shown. Note that the tetrahedral ClO_4^- anions are disordered at room temperature and are shown in two equivalent inversion related positions.

In order to discuss the very rich low-temperature physics of this material it is important to have a clear microscopic view of how the anion ordering affects the different parameters of the electronic structure. For instance, the interaction between the delocalized electrons of the donors and the localized charges of the anions in Bechgaard salts is usually believed to occur through direct Coulomb interactions between the charged anion and the nearby selenium atoms of the donors [24] (see Fig. 1), which polarize the π type HOMO of the donors and thus affect the band structure [25]. However, we have recently proposed that a second plausible mechanism, mediated by the hydrogen bonds of the lattice, may be also at work [18]. For instance, such a mechanism has been shown to be essential in understanding the long-debated charge ordering transition of α -(BEDT-TTF) $_2\text{I}_3$ [16].

The anion ordering in both $(\text{TMTSF})_2\text{ClO}_4$ [20,21] [$T_{AO} = 24$ K, $Q_{AO} = (0, 1/2, 0)$] and $(\text{TMTSF})_2\text{NO}_3$ [26,27] [$T_{AO} \sim 43$ K, $Q_{AO} = (1/2, 0, 0)$] results with a doubling of the unit cell. However, whereas such doubling occurs along the interchain direction (i.e., b) in $(\text{TMTSF})_2\text{ClO}_4$, it occurs along the intrachain direction (i.e., a) in $(\text{TMTSF})_2\text{NO}_3$. Thus, comparison of these two salts offers an excellent opportunity to deepen our microscopic understanding of how the anion ordering influences the low-temperature electronic structure of these salts. In addition, $(\text{TMTSF})_2\text{NO}_3$ is an interesting salt with its own distinctive physics among Bechgaard salts. For instance, it is the only of these salts which does not become superconducting down to 50 mK under pressure [28]. It is also worth noting that the anion ordering seems to have a minor influence on the electronic properties of this system even if it stabilizes the $2k_F = a^*/2$ periodicity in the stack direction (surprisingly this $2k_F$ anion ordering transition is followed by a better rate of increase of the conductivity [29]; a feature which points out the relevance of the warping of the Fermi surface at low temperature in the Bechgaard salts).

We report here a first-principles DFT study of the electronic structure of these two salts, paying special attention to the subtle changes occurring as a result of the anion ordering transitions, and show that many of the questions concerning the electronic structure above and below the ordering can be simply rationalized on the basis of these calculations.

II. COMPUTATIONAL DETAILS

The present calculations were carried out using a numerical atomic orbitals DFT approach [30,31], which was developed for efficient calculations in large systems and implemented in the SIESTA code [32–35]. We have used the generalized gradient approximation (GGA) to DFT and, in particular, the functional of Perdew, Burke, and Ernzerhof [36]. Only the valence electrons are considered in the calculation, with the core being replaced by norm-conserving scalar relativistic pseudopotentials [37] factorized in the Kleinman-Bylander form [38]. We have used a split-valence double- ζ basis set including polarization orbitals with an energy shift of 10 meV for all atoms [39]. The energy cutoff of the real space integration mesh was 250 Ry. The Brillouin zone was sampled using a grid of $(20 \times 10 \times 5)$ k points [40] in the irreducible part of the Brillouin zone for determination of density matrix and a set of $(31 \times 31 \times 6)$ k points for the determination of the Fermi surface. The experimental room-temperature and ambient-pressure crystal structure of Gallois [41], the 7 K and ambient-pressure anion ordered and average structures of Le Pévelen *et al.* [21,42], and the 7 K and 5-kbar crystal structure of the same authors [21,42] were used in the calculations for $(\text{TMTSF})_2\text{ClO}_4$. The calculations for $(\text{TMTSF})_2\text{NO}_3$ were based on the room temperature, 12 K average, and 12 K anion ordered crystal structures reported by Hebrard-Bracchetti *et al.* [27,43].

III. ELECTRONIC STRUCTURE OF $(\text{TMTSF})_2\text{ClO}_4$

In this and the next section we describe the main results of the first-principles calculations and we postpone to the Discussion section a detailed comparison with the available experimental information concerning the physical behavior of these salts. The calculated band structure near the Fermi level for the room-temperature structure of $(\text{TMTSF})_2\text{ClO}_4$ is shown in Fig. 2(a). The two bands are almost exclusively built from the HOMO of TMTSF and because of the stoichiometry they contain one hole so that the upper band is half filled. The main parameters of the band structure are shown in the figure together with those for the 7 K average structure. In order to consider the effect of pressure we have also included the parameters for the 7 K and 5-kbar structure. There is a pair of dispersive bands along the chain direction with a total dispersion around 0.8 eV and exhibiting a dimerization gap at X of approximately 10% of the total dispersion. The two bands exhibit quite different dispersion along the b^* interchain direction, the upper one being considerably flatter. These features are shared with the previously published band structures both first-principles and extended Hückel [5,8,44,45]. The effect of thermal contraction is clear from the comparison of the room-temperature and 7 K average structures at ambient pressure: There is an increase of $\sim 11\%$ in the total dispersion

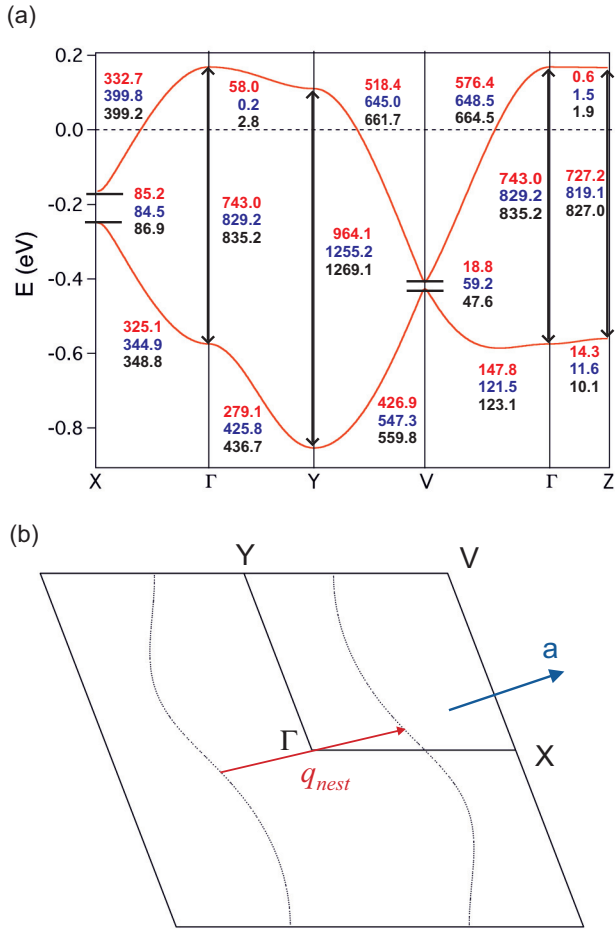


FIG. 2. (Color online) (a) Calculated band structure for $(\text{TMTSF})_2\text{ClO}_4$ without anion ordering. The main parameters of the band structure are shown for the room-temperature crystal structure (top, red values), the 7 K average structure (middle, blue values), and the 7 K and 5-kbar structure (bottom, black values). The energy zero corresponds to the Fermi level. $\Gamma = (0,0,0)$, $X = (1/2,0,0)$, $Y = (0,1/2,0)$, $Z = (0,0,1/2)$, and $V = (1/2,1/2,0)$ in units of the triclinic reciprocal lattice vectors. (b) Calculated $c^* = 0.0$ section of the Fermi surface for the 7 K average structure. Note that the nesting vector, q_{nest} , of the Fermi surface is nearly parallel to the stacks direction, a .

along the chains direction, whereas the dispersion along the b^* interchain direction considerably decreases for the upper partially empty band, which becomes almost completely flat, but considerably increases for the lower completely filled band. The dimerization gap at X is left almost unaltered. Judging from the values at 7 K for the 5-kbar and the ambient-pressure average structures, pressure has a very small effect on the parameters of the band structure. When compared with similar calculations for $(\text{TMTSF})_2\text{PF}_6$ at room temperature and ambient pressure [46], we note that the dispersion of the partially filled band along the c^* interlayer direction is around six times smaller for $(\text{TMTSF})_2\text{ClO}_4$ and is still smaller under 5 kbar. The calculated Fermi surface for the 7 K average structure is shown in Fig. 2(b).

The calculated band structure for the anion ordered structure at 7 K is shown in Fig. 3. It should be noted that this

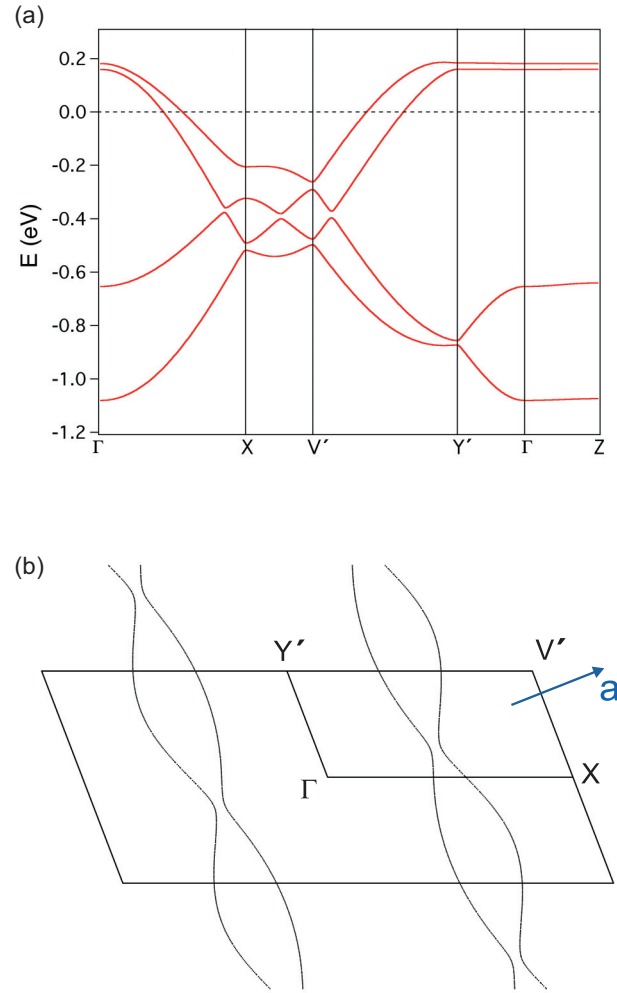


FIG. 3. (Color online) Calculated band structure (a) and $c^* = 0.0$ section of the Fermi surface (b) for the anion ordered structure of $(\text{TMTSF})_2\text{ClO}_4$ at 7 K. The energy zero corresponds to the Fermi level. $\Gamma = (0,0,0)$, $X = (1/2,0,0)$, $Y' = (0,1/2,0)$, $Z = (0,0,1/2)$, and $V' = (1/2,1/2,0)$ in units of the triclinic reciprocal lattice vectors of the $a \times 2b \times c$ superlattice. Note that the anion ordering gap occurs practically along the stacks direction, a .

calculation converges very slowly and a large set of k points to sample the Brillouin zone must be used in order to ensure that the results are really converged. This band structure is very similar to that recently reported by Nagai *et al.* [23] However, when the Fermi surface is calculated [see Fig. 3(b)], it is found that the two components of each pair of lines of the Fermi surface are definitely separated. Since special care was taken in ensuring that the results are converged we conclude that there is an anion ordering band gap. Our calculated value for this gap ($2\Delta_{AO}$) is 28.7 meV, which thus gives a value of ~ 14 meV for the half gap, Δ_{AO} . From now on we refer to Δ_{AO} as the anion ordering gap. The separation between the two lines of the Fermi surface is certainly smaller than found in the tight-binding calculations [21], but according to our calculations there is no doubt about its occurrence. The Fermi surface in Fig. 3(b) exhibits two important differences with a purely folded version by $b^*/2$ of that in Fig. 2(b): (i) The separation between the two components of each pair

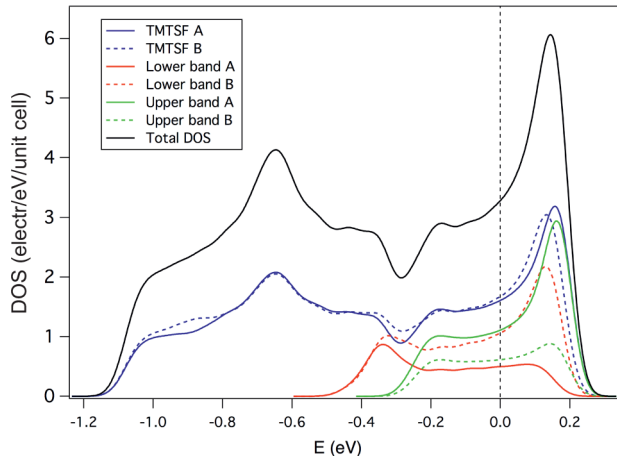


FIG. 4. (Color online) Total and projected density of states (PDOS) associated with the two different TMTSF donors in the anion ordered structure of $(\text{TMTSF})_2\text{ClO}_4$. Also shown are the individual contributions to each of the two partially filled bands.

increases when the b^* component increases along the direction perpendicular to a [see Fig. 3(b)], and (ii) the two components have different shape, one being flatter. Thus, the nesting between the two components of the Fermi surface has been deteriorated as a result of the anion ordering. To complement the DFT calculation, we present in the Appendix a simple model of the electronic structure and Fermi surface of the anion ordered state.

As mentioned, the anion ordering leads to a cell doubling along the interchain b direction. Consequently, two different types of TMTSF chains (A and B) alternate in the donor lattice after the ordering. We must now evaluate how different the two chains are in terms of the density of holes. The total and projected densities of states (PDOS) associated with the two types of TMTSF donor molecules are shown in Fig. 4. It is clear from the PDOS curves that the ordering leads to a small differentiation between the two donors. The calculated values for the partition of holes obtained through integration of these curves are $+0.522$ for donors A and $+0.478$ for donors B. Thus, the charge transfer between chains A and B is quite small, although it follows the same trend as the deformations of the TMTSF donors. Note that the small charge transfer is consistent with the fact that the anion ordering gap is not very large (see the Appendix).

At this point it is important to consider in a more precise way how the anions influence the electronic structure of the donor layers. In order to do so we have carried out two different calculations with exactly the same computational details used for the converged calculation. In the first one, the ClO_4^- anions are completely removed from the calculation and the neutrality of the system is enforced by using a uniform background of charge amounting to two electrons per unit cell. In this calculation the effect of the anion is thus only represented through the deformations induced in the TMTSF layers by the anion ordering. In the second calculation, the ClO_4^- anion was replaced by a spherical ion (i.e., a Cl^-). In such a way there is a negative charge located at the place of the anion but without directional properties as in the ClO_4^- anions. The calculated

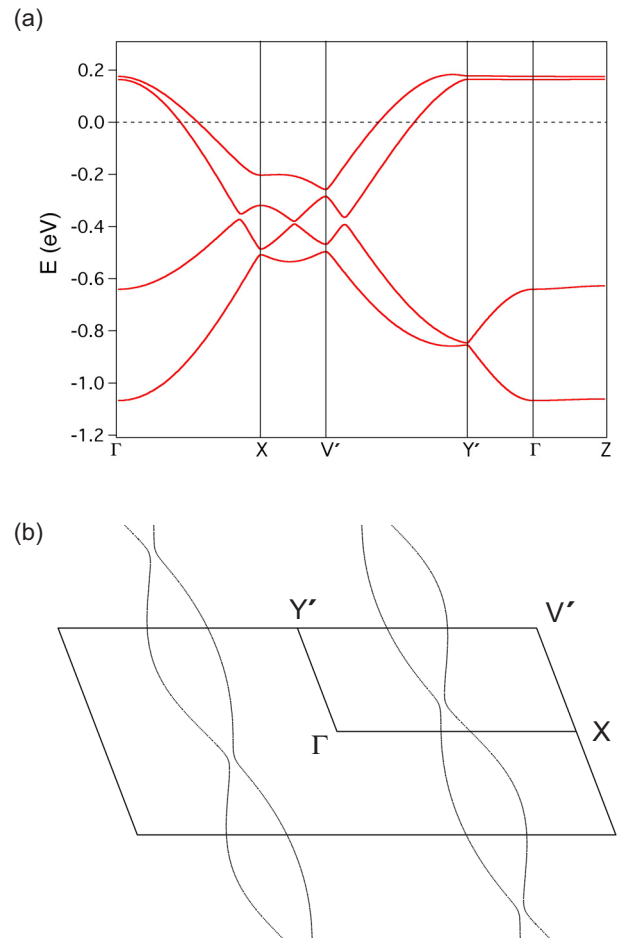


FIG. 5. (Color online) Calculated band structure (a) and $c^* = 0.0$ section of the Fermi surface (b) for the anion ordered structure of $(\text{TMTSF})_2\text{ClO}_4$ at 7 K when the anions were completely removed from the calculation and replaced by a uniform background of charge to keep electroneutrality. The energy zero corresponds to the Fermi level. $\Gamma = (0,0,0)$, $X = (1/2,0,0)$, $Y' = (0,1/2,0)$, $Z = (0,0,1/2)$, and $V' = (1/2,1/2,0)$ in units of the triclinic reciprocal lattice vectors of the $a \times 2b \times c$ superlattice.

band structure and Fermi surface obtained when the uniform background charge was used are shown in Fig. 5; the results of the second calculation were almost the same. Practically no change is noticed in the band structure, especially in the region around the Fermi level and, consequently, the Fermi surface is also very similar [see Fig. 5(b)], exhibiting only a slight reduction of the gap between the two sheets. The calculated anion ordering gap, Δ_{AO} , when the anions are removed is 9.7 meV so that the gap decreases by less than one-third, in contrast with most of the assumptions concerning this point in the literature. This suggests that the correct way to take into account the effect of the anion ordering on the band structure is mostly through the structural deformations induced in the TMTSF layers (a modulation of the dimerization) and not simply through the Coulomb potential of the anions, as it has been almost invariably assumed.

The small difference in the density of holes calculated for the two TMTSF donors (see Fig. 4, blue lines) could be taken as indicative of a very weak effect of the anion ordering in

the partially filled bands of the salt. However, this would be incorrect. In Fig. 4 we also show the contribution of the two different TMTSF donors for each of the two partially filled bands. The green and red curves are those associated with the upper and lower partially filled bands, respectively, whereas the solid and dashed lines correspond to TMTSF A and B, respectively. The difference between the solid and dashed lines of each color is very clear, the difference at the Fermi level being approximately one-third of the total value. This means that the two partially filled bands at the Fermi level are considerably polarized. Quantitative evaluation of the participation of the each TMTSF HOMO to the DOS at the Fermi level associated with each partially filled band leads to the values 32% (TMTSF A) and 68% (TMTSF B) for the lower band and 65% (TMTSF A) and 35% (TMTSF B) for the upper band. As discussed below, this polarization could have important consequences for the physical behavior of $(\text{TMTSF})_2\text{ClO}_4$.

The previous discussion suggests that the flatter line of the Fermi surface is preferentially associated with the chains of TMTSF B, whereas the more warped one is preferentially associated with those of TMTSF A. There is another important modification of the band structure as a result of the anion ordering. Looking at the X point of the band structure of Fig. 3(a) (and disregarding the slightly avoided crossings along $\Gamma \rightarrow X$), one observes the occurrence of two very distinct dimerization gaps. The larger gap is associated with the top partially filled band and, consequently, is related to the dimerization in the TMTSF A chains; the second gap is associated with the lower partially filled band and, consequently, is related to the dimerization in the TMTSF B chains. Of course, the two gaps are of the same order when the 7 K average structure is used. Thus, these calculations clearly show that the anion ordering leads to a modulation of the dimerization in successive chains which is intimately related to the relocation of the electronic states around the Fermi level.

Such modulation of the dimerization has already been recognized by Le Pévelen *et al.* [21] on the basis of the variation of the corresponding transfer integrals. According to these authors, it results from the difference in site energy between donors A and B and the molecular deformations of the central part of the donors. However, the variation of the site energy as a result of the different charges cannot lead to a change in the dimerization because every chain contains only one type of donor. Thus, the effect of the molecular deformations of the central part of the TMTSF, though so far not clarified through what mechanism, seems to provide a more likely origin. However, one must then reconcile this feature with the small calculated difference of charges, which are also considered to result from the deformation of the central core of TMTSF. Note also that the interplanar spacing in the anion ordered structure is the same for the two chains according to the crystal structure study by Le Pévelen *et al.* [21]. A satisfactory explanation should take into account all these observations. The effect can be understood on the basis of the hydrogen-bond-mediated mechanism for donor-anion interaction. As shown in Fig. 6, the anion ordering in $(\text{TMTSF})_2\text{ClO}_4$ is accompanied by a shift of the anions towards the chains of donors A. This leads to an increase of

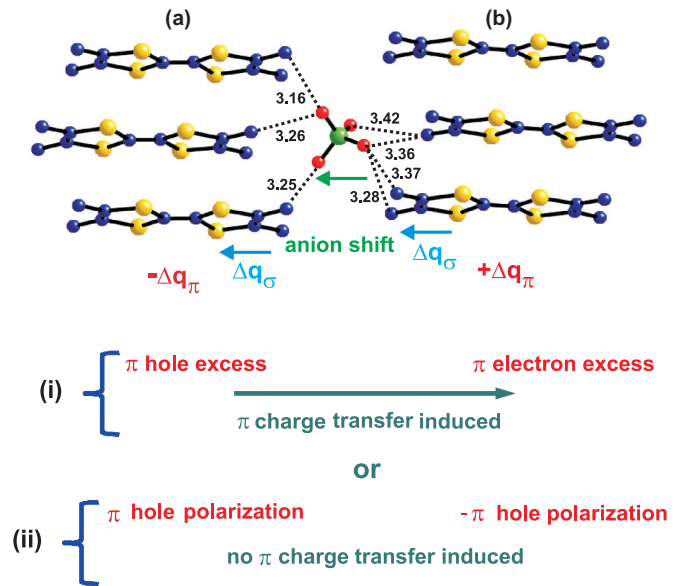


FIG. 6. (Color online) Illustration of the possible consequences for the donors π electron system of the anions decentering inside the methyl groups cavity during the anion ordering transition of $(\text{TMTSF})_2\text{ClO}_4$ ($\text{C} \cdots \text{O}$ contacts up to 3.45 Å are shown).

the hydrogen bonding interaction between the methyl groups of donor A and the anion. In fact, whereas the carbon atoms of the methyl groups in donor B remain planar after the anion ordering, those of donor A move noticeably away from the mean plane on opposite sides [21], a clear sign of the increase of the hydrogen bonding interactions. As proposed before [16,18], an increase of the strength of the hydrogen bonding between the terminal methyl or ethyl hydrogens of the donor and a neighboring anion makes these terminal hydrogens more positively charged and induces a negative σ charge shift towards the inner part of the donor (see Fig. 6). Consequently, a more positive charge in the inner π system is stabilized. If there is some connection (i.e., if there is a non-negligible transfer integral) with the neighboring donors, the shift may result in a transfer of holes from one donor to the other [case (i) in Fig. 6]. This is the case for the charge ordering transition in α -(BEDT-TTF) $_2\text{I}_3$ [16]. However, if the connection with neighboring donors is less effective (for instance, because of smaller transfer integrals or symmetry restrictions of the lattice), then the π system will simply polarize so that a larger concentration of holes will occur in the donor moiety nearest to the anion [case (ii) in Fig. 6]. In that case there is no charge transfer but the donor can still distort because the polarization is decreasing or increasing the π electron density in certain bonds. Thus, there is no contradiction in having small charge transfer but geometrical changes in the central part of the donor. In the present case, the anion ordering occurs in such a way that all donors of one chain are symmetry equivalent so that there is no intrachain charge transfer. In addition, as shown by the very small dispersion of the two upper bands after the anion ordering (see Fig. 3), the interchain interactions must be very small. Consequently, there is a small charge transfer between the two donors but there are nevertheless important changes on the electronic structure of the systems, as revealed

by our calculations. The polarization of the HOMO and the zigzag nature of the chains leads to an increase of the transfer integrals along the chains but the effect is stronger when the polarization of the π system of the central part is stronger, i.e., for the chain making the stronger hydrogen bonds. This is why even if there is a small interchain charge transfer, the central C=C bond is longer for donor A (0.034 Å) and the dimerization in the chains of this donor is larger.

IV. ELECTRONIC STRUCTURE OF (TMTSF)₂NO₃

The calculated band structure near the Fermi level for the room-temperature structure of (TMTSF)₂NO₃ is shown in Fig. 7(a). Apparently, this band structure is different from all other known band structures for Bechgaard salts in that just at the Fermi level there is a flat band hybridizing with the usual band. However, this result has no physical meaning. It is simply due to the fact that the NO₃ anion contains one NO bond unreasonably short (1.07 Å) in the room-temperature crystal structure [27,43], which artificially raises one of the electronic levels of the anion. However, the donor sublattice seems to be correctly described in this crystal structure. In view of the results of the previous section we have recalculated the band structure removing the anions and using a uniform background charge. This band structure, reported in Fig. 7(b), is identical to the previous one once the spurious flat band is removed so that we propose that, as far as the bands near the Fermi level are concerned, the band structure of Fig. 7(b) provides the correct description for (TMTSF)₂NO₃ at room temperature. The main parameters of the band structure, as well as those for the 12 K average structure, are included in Fig. 7(b). As usual, thermal contraction leads to an increase of most of these parameters but we note a difference with (TMTSF)₂ClO₄. Whereas the band dispersion along the $\Gamma \rightarrow Y$ direction at room temperature is very similar in both salts, for (TMTSF)₂ClO₄ the dispersion for the upper band is almost nil at low temperature (both with or without pressure), whereas it does practically not change for (TMTSF)₂NO₃. This points out to a clearly different variation with temperature of the interchain interactions in the two salts (see the discussion in Sec. V). The calculated Fermi surface for the 12 K average structure (i.e., without anion ordering) is shown in Fig. 7(c). The band structure around the Fermi level and Fermi surface calculated without the anions and the uniform background charge are identical with those of this figure.

The calculated band structure for the 12 K anion ordered structure is shown in Fig. 8(a). In the lower part of the HOMO bands, around -0.8 eV, a flat band located on the anion appears and hybridizes with the donor bands. In contrast with the case of the room-temperature crystal structure, this is a real feature. However, this band occurs too far from the Fermi level to have a role in the physics of this system. Shown as dashed lines, the calculated band structure when the anions are removed is also plotted in Fig. 8(a). Again it is concluded that the main effect of the anion ordering on the band structure occurs through the deformations induced in the TMTSF layers. The calculated Fermi surface after the anion ordering is shown in Fig. 8(b). This Fermi surface is simply a folded version by $a^*/2$ of that of Fig. 7(c) with small gaps around the crossing points of the high-temperature Fermi surface. It thus contains hole pockets

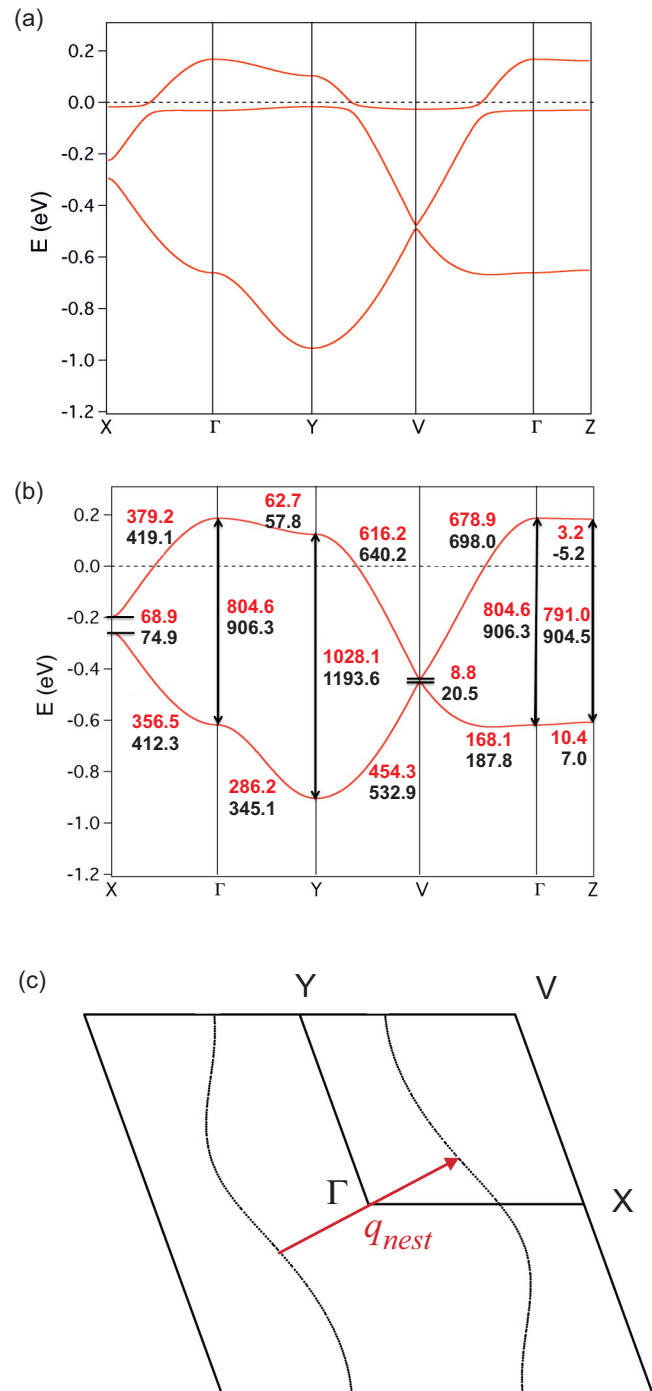


FIG. 7. (Color online) (a) Calculated band structure for (TMTSF)₂NO₃ using the room-temperature crystal structure. (b) Calculated band structure for (TMTSF)₂NO₃ using the room-temperature crystal structure where the anions were completely removed and replaced by a uniform background charge. The main parameters of the band structure are shown for this calculation (top, red values) and for the full calculation using the 12 K average structure (bottom, black values). The negative values are used to indicate a slope opposite to that usually shown by the dispersion. $\Gamma = (0,0,0)$, $X = (1/2,0,0)$, $Y = (0,1/2,0)$, $Z = (0,0,1/2)$, and $V = (1/2,1/2,0)$ in units of the triclinic reciprocal lattice vectors. (c) Calculated $c^* = 0.0$ section of the Fermi surface for the 12 K average structure. The nesting vector of the Fermi surface, q_{nest} , is also indicated.

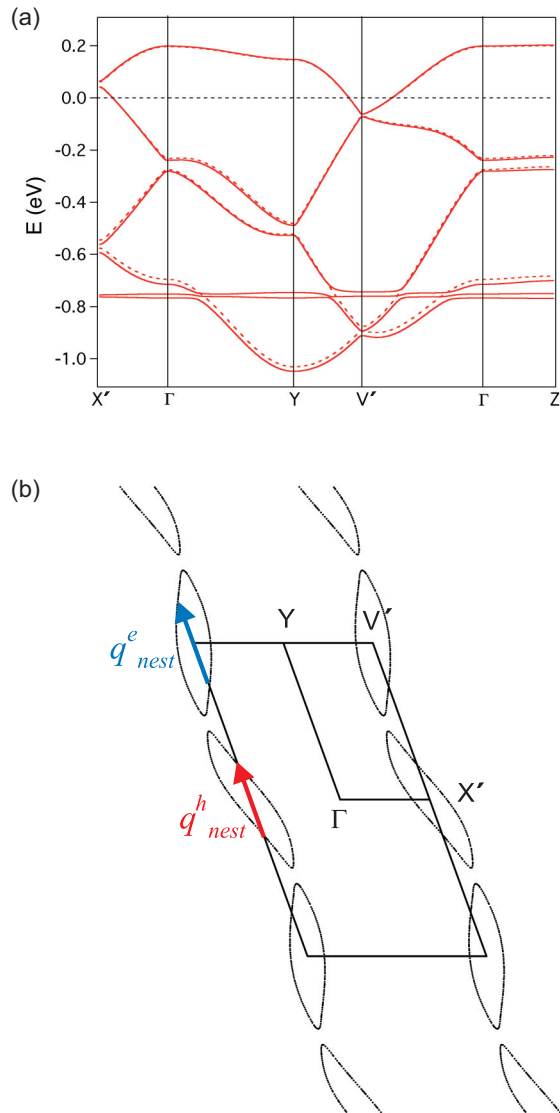


FIG. 8. (Color online) Calculated band structure (a) and $c^* = 0.0$ section of the Fermi surface (b) for the anion ordered structure of $(\text{TMTSF})_2\text{NO}_3$ at 12 K. The dashed lines in (a) are the bands calculated when the anions were substituted by a background uniform charge. The energy zero corresponds to the Fermi level. $\Gamma = (0,0,0)$, $X' = (1/2,0,0)$, $Y = (0,1/2,0)$, $Z = (0,0,1/2)$, and $V' = (1/2,1/2,0)$ in units of the triclinic reciprocal lattice vectors of the $2a \times b \times c$ superlattice. Note that the anion ordering gaps which develop at $\pm b^*/4$ leave unaffected the flat parts of the dispersion of the hole pockets (around $-b^*/8$ and $+b^*/8$) and of the hole pockets (around $+3b^*/8$ and $+5b^*/8$).

around X' and electron pockets around V' . The area of these pockets is calculated to be 5.8% of the cross section area of the Brillouin zone. The calculated anion ordering gap Δ_{AO} , 8.9 meV, is smaller than that found for $(\text{TMTSF})_2\text{ClO}_4$. When the anions are removed from the calculation the gap decreases by 21.7%.

We must now consider the distribution of holes among the two donors. The central $\text{C}=\text{C}$ distances differ by 0.035 \AA with that for TMTSF A being longer, according to the 12 K crystal structure [43]. This is practically the same difference found for

$(\text{TMTSF})_2\text{ClO}_4$ (0.034 \AA) [21]. Despite this, our calculation leads to somewhat larger charges, $+0.540$ for TMTSF A and $+0.460$ for TMTSF B. This is consistent with our analysis of the transfer of charge in $(\text{TMTSF})_2\text{ClO}_4$ because now the anion ordering occurs along the direction of the chains so that the intrachain charge transfer is possible. The fact that even in that case the magnitude of the charge transfer is smaller than that calculated for α -(BEDT-TTF) $_2\text{I}_3$ [16], is most likely due to the fact that the alkyl groups hydrogen bonded to the anions in BEDT-TTF is adjacent to a more polarizable sulfur atom. Consequently, the negative σ charge shift towards the inner part of the donor is more effectively transmitted. When the contribution of the each TMTSF HOMO to the DOS at the Fermi level associated with each of the two partially filled bands is calculated, the following values are obtained: 39% (TMTSF A) and 61% (TMTSF B) for the lower band and 59.4% (TMTSF A) and 40.6% (TMTSF B) for the upper band. The values for each band are less different than those for $(\text{TMTSF})_2\text{ClO}_4$. Consequently, the anion ordering in this case leads to a larger charge transfer between the two donors but to a smaller polarization of the two partially filled bands. This is understandable since the donors are more tightly bonded to ClO_4^- than NO_3^- so that it is expected that the polarization effect is stronger for the first anion. However, the hole transfer between the two types of donors is associated with the interchain interactions in the first salt but with the intrachain interactions, which are one order of magnitude larger, in the second salt.

A final point we must examine is that of the actual change of the donor-anion interactions when the anion ordering occurs. As discussed above, when charge or anion ordering transitions develop, there is an increase of the hydrogen bonding interactions between the anions and the peripheral hydrogen atoms of part of the donors which, via a double polarization mechanism [16,18] (see Fig. 6), stabilize a π hole excess and/or a π hole polarization on these donors. In other words, anion shift and anion reorientation towards a donor render it more positively charged below the anion ordering transition. Is such a hydrogen-bonding-mediated mechanism also at work here? The shorter hydrogen bonds ($\text{O} \cdots \text{H}$ contacts up to 2.6 \AA) between the anion and the two different TMTSF donors in the 12 K anion ordered structure of $(\text{TMTSF})_2\text{NO}_3$ are shown in Fig. 9. Clearly, TMTSF A, which is the more positively charged donor, is associated with the shorter donor-anion hydrogen bonds. Consequently, $(\text{TMTSF})_2\text{NO}_3$ provides a

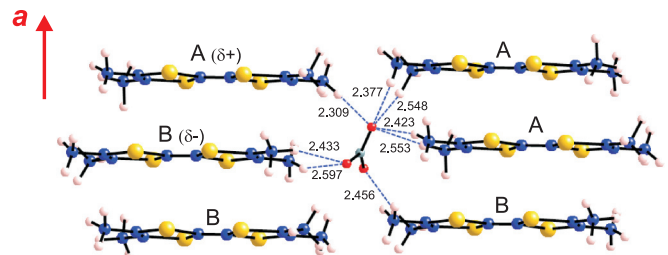


FIG. 9. (Color online) Short $\text{O} \cdots \text{H}$ contacts between the anion and the two different TMTSF donors in the anion ordered structure of $(\text{TMTSF})_2\text{NO}_3$ ($\text{O} \cdots \text{H}$ contacts up to 2.6 \AA are shown).

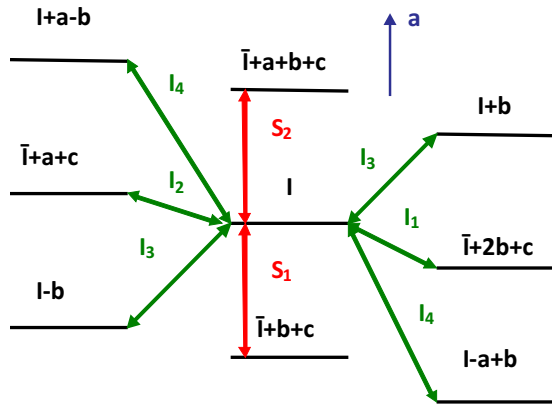


FIG. 10. (Color online) Schematic view of the packing in the (a,b) TMTSF donor layers of $(\text{TMTSF})_2X$ Bechgaard salts (see Fig. 1), where every TMTSF is represented as a thick black line and the symmetry operations relating the central TMTSF (I) to the other donors are indicated (\bar{I} refers to a TMTSF related by inversion symmetry to the central one). The different intrachain (red, S_1 and S_2) and interchain (green, I_1, \dots, I_4) transfer integrals are labeled.

further example of the hydrogen-bond-mediated mechanism at work.

V. DISCUSSION

The electronic structure of the $(\text{TMTSF})_2X$ salts is usually described on the basis of a 2D tight-binding model based on six different transfer integrals, t_{S1} and t_{S2} and $t_{I1}-t_{I4}$ (see Fig. 10). This description can be simplified by using the three transfer integrals model of Yamaji *et al.* [3,47], which introduces t_a , the average transfer integral along a , t_b^+ , the effective transfer integral between equivalent molecules related by b and $a+b$ translations, and t_b^- , the effective transfer integral between inversion related molecules nearly along the diagonal $b-a/2$ directions (see Fig. 10). The relationship between these transfer integrals and the t_{S_i} and t_{I_i} ones is explicitly given in Ref. [48]. This model gives a dispersion relation of the type $E(k) = 2t_a \cos(ka/2) + 2t_b \cos[kb + (-/+)\Phi]$ with the $(-/+)$ sign for $ka > 0$ and $ka < 0$, respectively, and t_b and Φ related to t_b^+ and t_b^- as defined in Ref. [48]. This dispersion relation leads to the definition of the optimal nesting wave vector of the Fermi surface (that linking the inflexion points

of its transverse dispersion) as $q_{\text{nest}} = [2k_F, (\pi + 2\Phi)/b]$ with the transverse component $q_{\perp} = [0.5 + (\Phi)/\pi]b^*$. In order to simplify the discussion and the comparison with previous data we have fitted our first-principles calculations to this tight-binding model. The fitted transfer integrals and band structure parameters t_a , t_b , and Φ are reported in Table I, as well as the transverse component, q_{\perp} , of the best nesting wave vector of the Fermi surface (note that in these expressions Φ is given in radians).

It is interesting to compare the calculated t_a and t_b values in Table I with those obtained from optical measurements for $(\text{TMTSF})_2\text{ClO}_4$ at 10 K [49], which led to the values $t_a = 0.3$ eV and $t_b = 40$ meV. t_a is comparable to the calculated value for the 7 K average structure (0.26 eV), while t_b is 20% smaller than the calculated value (~ 50 meV). One of the more notable differences between $(\text{TMTSF})_2\text{ClO}_4$ and $(\text{TMTSF})_2\text{NO}_3$ is the variation of the t_a/t_b ratio from room temperature to low temperature. For $(\text{TMTSF})_2\text{ClO}_4$, however, it decreases by 19%; for $(\text{TMTSF})_2\text{NO}_3$ there is practically no change. The increase of both t_a (22%) and t_b (36%) is larger for $(\text{TMTSF})_2\text{ClO}_4$ than it is for $(\text{TMTSF})_2\text{NO}_3$ (14% and 15%, respectively), but the average interchain interaction t_b increases more in $(\text{TMTSF})_2\text{ClO}_4$, leading to the decrease of the t_a/t_b ratio. Although these values clearly indicate a smaller influence of thermal contraction on the electronic structure of $(\text{TMTSF})_2\text{NO}_3$, one must be careful and look in more detail at the anisotropy of the transverse interactions by considering the evolution of t_b^+ and t_b^- previously defined. Only then can the details of the band structure and Fermi surface be clearly understood. The values of t_b^+ (t_b^-) (in meV) for ambient-pressure $(\text{TMTSF})_2\text{ClO}_4$ at room temperature and 7 K are 42.2 (-27.1) and 53.5 (-53.2), respectively. Because of the different sign of the TMTSF HOMOs of the dimer in the two bands, the two contributions add for the upper band but subtract in the lower band. Thus, at room temperature, the two bands exhibit dispersion, although considerably smaller for the upper, partially filled one. At low temperature, the two contributions practically cancel, leading to an almost nil dispersion for the partially filled band [see Fig. 2(a)]. The values of t_b^+ (t_b^-) for ambient-pressure $(\text{TMTSF})_2\text{NO}_3$ at room temperature and 12 K are 43.6 (-27.9) and 50.3 (-35.9), respectively. In that case, the two components change by almost the same amount so that the dispersion of the upper band does not vary considerably with temperature [see Fig. 7(b)].

TABLE I. Tight-binding transfer integrals fitted to the present first-principles calculations and band structure parameters for $(\text{TMTSF})_2\text{ClO}_4$ and $(\text{TMTSF})_2\text{NO}_3$. The transfer integrals are given in meV, Φ in degrees, and q_{\perp} in units of b^* .

	t_{S1}	t_{S2}	t_{I1}	t_{I2}	t_{I3}	t_{I4}	t_a	t_b	t_a/t_b	Φ	q_{\perp}
$(\text{TMTSF})_2\text{ClO}_4$ 300 K 1 bar	227.6	201.6	-19.3	-35.9	47.4	-5.2	213.4	35.8	6.0	-40.7	0.27
$(\text{TMTSF})_2\text{ClO}_4$ average structure 7 K 1 bar	278.5	242.6	-50.1	-56.4	55.9	-2.4	260.5	48.6	5.4	-67.3	0.13
$(\text{TMTSF})_2\text{ClO}_4$ 7 K 5 kbar	279.8	246.2	-49.3	-59.1	58.2	-3.2	263.0	49.7	5.3	-66.5	0.13
$(\text{TMTSF})_2\text{NO}_3$ 300 K 1 bar	238.8	219.4	-20.4	-35.4	55.5	-11.9	229.1	36.8	6.2	-39.5	0.28
$(\text{TMTSF})_2\text{NO}_3$ Average structure 12 K 1 bar	274.4	250.5	-29.1	-42.7	56.6	-6.3	262.5	42.3	6.2	-45.6	0.25

Such different evolution of the upper, partially filled, band thus results from the different variation of the anisotropy in the interchain interactions, which obviously also leads to a clearly different evolution of the transverse component of the nesting wave vector through the variation of the angle Φ (see Table I): almost no variation for $(\text{TMTSF})_2\text{NO}_3$ but reduction by one-half for $(\text{TMTSF})_2\text{ClO}_4$. Note that the t_b^+ (t_b^-) values for the two salts at room temperature are very similar. A look at Table I shows that the two interactions along b - $a/2$ between molecules related through an inversion center (t_{I1} and t_{I2}) in $(\text{TMTSF})_2\text{NO}_3$ change only by one-third of the variation in $(\text{TMTSF})_2\text{ClO}_4$ and this makes all the difference. Ultimately, this is the reason for the different wave vector of the low-temperature SDW ground state of the two salts. The values in Table I provide a simple way to describe the details of the first-principles calculations and thus are used in the following to analyze the low-temperature physics of these salts.

A. Anion ordering in $(\text{TMTSF})_2\text{ClO}_4$

As briefly mentioned above, anions exert a strong control on the physical behavior of $(\text{TMTSF})_2\text{ClO}_4$. The kinetics of anion ordering is slow, so that, depending on the cooling rate around the temperature where the anion ordering occurs, the low-temperature electronic properties may drastically differ [6,22]. In addition, the anion ordering temperature, T_{AO} , increases with pressure up to 41 K at 11 kbar, while the strength of the transition, as indicated by the magnitude of the resistivity anomaly, is reduced [50]. This kind of behavior has been usually rationalized assuming an inhomogeneous model in which anion ordered domains exhibiting superconductivity coexist with nonanion ordered domains exhibiting a SDW ground state [51]. However, such explanation has been recently questioned [52]. The current view of the superconductivity vs SDW interplay in this material is that the cooling rate controls the fraction of ordered anions and thus the anion ordering gap for which two limiting cases can be considered. First, the gap is nil or very small; i.e., there is no anion ordering. In that case, Fermi surface nesting leads to a SDW instability, resulting in the destruction of the Fermi surface and the concomitant metal-insulator transition. Second, the gap is very substantial. In that case, the nesting is spoiled so that the SDW is not stabilized and superconductivity occurs. An interesting question within this scenario is thus as follows: Do SDW and superconductivity coexist or compete for intermediate values of the gap?

Clearly, a prerequisite for a better understanding of the low-temperature behavior of $(\text{TMTSF})_2\text{ClO}_4$ is to have a realistic estimation of the magnitude of the anion ordering gap (see the Appendix for the development of simple models). Several experimental and theoretical works have faced this problem, although to the best of our knowledge there is not yet a clear consensus. All theoretical models assume that the anion ordering introduces an extra potential of the type $V(y) = V\cos(y\pi/b)$, i.e., a potential of the same strength but alternating sign for the successive chains of TMTSF A and B along b , and that only V leads to changes in the band dispersion below the anion ordering. The model assumes that there is no sizable change of the transfer integrals below the anion ordering. In other words, the new Fermi surface can be simply generated by a folding along b^* and the subsequent

opening of a gap $2V$ at the border of the Brillouin zone due to this extra potential (this model is revisited in the Appendix by taking into account the true oblique structure of the TMTSF array). However, as shown by the structural study of Le Pévelin *et al.* [21], there is a clear differentiation between two types of chains which must result in variations of the transfer integrals. Also, the first-principles results in Sec. III show that (i) a periodic anion potential V does not provide an appropriate way to model the effect of the anion ordering on the band structure, (ii) the anion ordering has important consequences for the band structure (variation of the dimerization of the chains, polarization of the partially filled bands, etc.), and (iii) the shape of the Fermi surface is quite different from that of the simple folded model since the minimum separation between the two lines occurs around the center (and not the border) of the Brillouin zone. Thus, the above-mentioned scenario does not seem to be really appropriate. In this context, the first-principles calculations can be of major value in answering questions such as the following. How large is the anion ordering gap? How does this gap influence the low-temperature electronic instabilities? How are the anion ordering and the possible nodal gap structure of the superconducting state in $(\text{TMTSF})_2\text{ClO}_4$ related?

1. SDW modulation in quenched $(\text{TMTSF})_2\text{ClO}_4$

Let us first consider the quenched samples for which a SDW transition occurs at 6 K [51] to 7 K [52]. The 7 K structure under 5 kbar reported by Le Pévelin *et al.* [21] corresponds to a quenched system because of the too-fast cooling rate employed. Superstructure reflections were not observed so that the structure is representative of a quenched sample and the electronic structure is like that of the high-temperature phase [see Fig. 2(a)]. According to the DFT calculations a nesting wave vector, q_{nest} , with transverse component of $0.13b^*$ [see Table I and Fig. 2(b)] is the best nesting vector of the Fermi surface. Note that this transverse component has decreased from $0.27b^*$ at room temperature because when lowering the temperature, the strength of the interactions between donors related through inversion (I1 and I2) increases faster than those between donors related by translation (I3 and I4). If we use instead the 7 K average structure at 1 bar the transverse component is also calculated to be $0.13b^*$. These values are in excellent agreement with the experimental determination of the SDW transverse component ($0.12b^*$) reported by Delrieu *et al.* [53,54] for quenched $(\text{TMTSF})_2\text{ClO}_4$. Previous tight-binding calculations led to similar values for the average 7 K structure, $q_{\perp} = 0.13b^*$ [55], and the 7 K and 5-kbar structure, $q_{\perp} = 0.17b^*$ [21]. In contrast, for the room-temperature and ambient-pressure structure a tight-binding study [55] led to a value of $0.38b^*$ for q_{\perp} , which is considerably larger than our value. However, the calculated value using the transfer integrals obtained in a previous DFT study [8] or those of a different tight-binding study [5], $q_{\perp} = 0.28b^*$ and $q_{\perp} = 0.29b^*$, respectively, are both in very good agreement with the present first-principles one.

2. Anion ordering gap in relaxed $(\text{TMTSF})_2\text{ClO}_4$

For relaxed samples the structural study of Le Pévelin *et al.* [21] shows that there are two different stacks alternating

along the interstacks b direction so that the Fermi surface splits into two components [see Fig. 3(b)]. The two key questions to ask are as follows. (i) How much do these two components separate? (ii) How large is $2\Delta_{AO}$? A simple model to tackle this problem is developed in the Appendix. The area between the two split Fermi surfaces calculated for the anion ordered phase [Fig. 3(b)] amounts to 4.8% of the (a^*, b^*) high-temperature Brillouin zone [4.55% for the folded Fermi surface of the average structure calculated in Fig. 2(b)]. This area can be experimentally estimated if under high magnetic field closed orbits are achieved by magnetic breakdown through the anion gap. Such a mechanism was proposed to account for the 255-T frequency of the Shubnikov-de Haas rapid oscillations measured for $(\text{TMTSF})_2\text{ClO}_4$ [56]. Such a frequency corresponds to 3.5% of the (a^*, b^*) high-temperature Brillouin zone, which amounts to about 73% of the calculated area. The difference is not dramatic because, as pointed out at the beginning of Sec. V, the DFT calculation overestimates t_b (and thus the pocket area) by about 25% (50 meV instead of 40 meV). Concerning the value of the anion gap, there are two different computational studies in the literature, both based on the above-mentioned crystal structure. A relatively large splitting of ~ 150 meV, essentially originating from the energy difference between HOMO_A and HOMO_B , can be deduced from the tight-binding extended Hückel calculations [21]. In contrast, a DFT study leads to a nil gap [23]. The present study leads to two pairs of Fermi surface lines split by 28 meV, i.e., a half-gap (Δ_{AO}) value of 14 meV.

There are several experimental-based estimations of the Δ_{AO} value (or more likely of V because the dispersion of the folded band structure has been used in the data interpretation) [57,58]. For instance, analysis of the rapid oscillations of the magnetoresistance led to a value of 4.5 meV [59], now corrected to 6 meV by using a Fermi energy based on our DFT calculations. Using the angular dependence of the magnetoresistance and more specifically the Third Angular Effect, several estimations have been proposed. For instance, Yoshino *et al.* [60] suggested values of $\sim 0.083t_a$ (or equivalently $\sim 0.83t_b$) later corrected [61] to $\sim 0.028t_a$ (or equivalently $\sim 0.34t_b$); Lebed *et al.* [62,63] estimated the value $\sim 0.20t_b$ and Yoshino and Murata [64] proposed the values $\sim 0.028t_a$ (or equivalently $\sim 0.17t_b$). It must be noted that these works used different values of t_a/t_b , in the range 12–6, which are larger than our estimated value at 7 K, 5.4. Using the t_a and t_b values of Table I it is found that the latter estimation by Yoshino *et al.*, ~ 7.3 meV ($0.028t_a$) [or ~ 8.3 meV ($0.17t_b$)], that by Lebed *et al.*, ~ 9.7 meV, as well as the corrected value by Uji *et al.* [59], are all within a small energy range of $\cong 6$ –10 meV, which is not far from our estimated value of 14 meV. Note that the DFT calculations slightly overestimate the transverse interactions. An optical study of $(\text{TMTSF})_2\text{ClO}_4$ at 10 K [49] gives a t_a/t_b value of 7.5, slightly larger than our calculated value of 5.4 but also smaller than the ratios assumed in the analysis of the latter experimental works. Thus, we believe that a value of 7–10 meV is a reasonable value for Δ_{AO} , consistent with most of the experimental and theoretical analyses. We definitely conclude that there is a small but non-nil anion ordering gap which, in any case, is clearly smaller than t_b .

3. Absence of SDW in relaxed $(\text{TMTSF})_2\text{ClO}_4$

This part addresses the following question: Why is there no SDW instability after anion ordering? Previous estimations of the electron-hole susceptibility suggest that the occurrence of the instability is controlled by the relative strength of the anion ordering potential (i.e., the anion ordering gap) with respect to the transverse dispersion, $4t_b$ [65–67]. If the gap is smaller than $4t_b$, it is found that the anion potential does not alter in a significant way the divergence of the response function. In contrast, when the gap is larger than $4t_b$ the divergence shades off. The analysis of the previous section clearly suggests that the anion ordering gap is smaller than $4t_b$, so that its magnitude cannot suppress the SDW instability.

The analysis of the electronic structure of $(\text{TMTSF})_2\text{ClO}_4$ in Sec. III suggested two potential reasons for the absence of SDW instability for finite, but small, values of Δ_{AO} : (a) the polarization of the wave functions at the Fermi level and (b) the warping of the Fermi surface after anion ordering.

The preferred localization of the wave functions associated with the two separate lines of the Fermi surface for the chains of TMTSF A or B should lead to a decrease of T_{SDW} via the reduction of the numerator in the Lindhard response function, which involves an overlap matrix associated with wave functions located in different chains. However, a realistic estimation of such reduction leads to values of $\sim 1/2$ so that this feature alone cannot be at the origin of the suppression of the instability in that case.

The Fermi surface of Fig. 3(b) is made up of two pairs of separate lines with considerably different warping: The inner, less warped pair, which is more heavily based on the chains of TMTSF B, and the outer, more warped pair, which is more heavily based on the chains of TMTSF A. In that case, the inner Fermi surface poorly nests into the outer Fermi surface. If the nesting deterioration due to the different warping is taken into account via a $2t'_b \cos(2k_y b - 2\Phi)$ term where t'_b is the imperfect nesting hopping integral (see the Appendix for a more quantitative definition), it is possible to use the calculated Fermi surface of Fig. 3(b) to estimate that $t'_b/t_b \sim 0.2$. Then, the mean-field theory of the SDW transition [68] shows that the SDW phase disappears when $2t'_b$ is larger than the SDW Δ_0 half-gap which, according to optical measurements [69], has a value of ~ 4 meV for both $(\text{TMTSF})_2\text{PF}_6$ and $(\text{TMTSF})_2\text{ClO}_4$. Thus, $2t'_b \sim 0.4t_b \sim 20$ meV (from Table I) is larger than Δ_0 , so that the SDW cannot be stabilized in the anion ordered ground state. Thus, we suggest that the suppression of the SDW instability is mostly caused by the deterioration of the nesting due to the reconstruction of the band structure in the anion ordered ground state, whereas the polarization of the wave functions at the Fermi level seems to be only of minor importance.

It is worth noting that our estimation of t'_b is consistent with the reversal of the Hall coefficient observed in the field-induced SDW phases [70,71]. Hasegawa and Kishigi [67] have shown that this phenomenon occurs when the anion ordering gap is smaller than $2t'_b$, which is clearly the case for the Δ_{AO} values obtained in Sec. V A 2. The present analysis points out the difficulty to achieve the SDW instability in the anion ordered state because the nesting breaking transfer integral t'_b is an important fraction of t_b . To recover the

divergence of the SDW response function, the t'_b associated with the differential deformation of the type-A and type-B organic stacks should substantially decrease. Such decrease is experimentally achieved by applying a b' -axial elongation to $(\text{TMTSF})_2\text{ClO}_4$ in its anion ordered phase [72]. Indeed, under b' -axial elongation, the 1.2 K superconducting transition of relaxed $(\text{TMTSF})_2\text{ClO}_4$ is replaced by a metal-insulator phase transition around $T_{\text{SDW}} \sim 7$ K. This phase transformation, which is not observed under a -axial elongation, shows that the interchain interaction in the b' direction is a key parameter in controlling the phase diagram of $(\text{TMTSF})_2\text{ClO}_4$.

4. Nodal gap structure of the $(\text{TMTSF})_2\text{ClO}_4$ superconducting state

The present first-principles results provide a quite detailed understanding of the evolution of the Fermi surface of $(\text{TMTSF})_2\text{ClO}_4$ with temperature, and more particularly, through the anion ordering process. Here we would like to use these results to comment on the question of the nodal gap structure of the superconducting state of $(\text{TMTSF})_2\text{ClO}_4$. In this state the k dependence of the order parameter has more degrees of freedom than it has in the superconducting state of $(\text{TMTSF})_2\text{PF}_6$ because its sign can also change between the split pairs of the Fermi surface. In this context, either a nodeless d (or f)-wave-like state or a nodal d -wave-like state has been proposed [23,73,74]. In addition, a recent phenomenological model [75] based on a group theoretical analysis and on the available experimental data, suggests a fully gapped p -wave polar triplet state. The situation is also confusing concerning the experimental determination of the superconducting gap structure. Field-angle-resolved calorimetry measurements have provided evidence of nodal gap structure [76], while a fully gapped p -wave singlet odd-frequency pairing was proposed from magnetic penetration depth measurements [77].

As discussed in the previous sections, the Fermi surface of $(\text{TMTSF})_2\text{ClO}_4$ after anion ordering consists of two pairs of separated lines [see Fig. 3(b)]. The anion ordering induces a deformation of the TMTSF stacks such that two distinct types of stacks (A and B) alternate along the donor layers. Such anion ordering does not only lead to two separate lines of the Fermi surface but differently polarizes the wave functions associated with each sheet, so that the inner one is more strongly associated with the TMTSF B stacks, whereas the outer sheet is preferentially associated with the TMTSF A ones. Thus, the simplest description of the origin of the two Fermi surface sheets is to say that they result from the bonding and antibonding interaction between the two types of chains which are coupled through interchain interactions. This kind of bonding-antibonding coupling (i.e., with opposite sign) in Q1D systems leads to a minimum of separation between the two Fermi surface sheets near the center of the Brillouin zone (see, for instance, the case of the blue bronzes $A_{0.3}\text{MoO}_3$; $A = \text{K, Rb, Tl}$) [78,79]. In the present case, the minimum is found for $k_b \approx \pm 0.12b^*$ with $b^* = 1/2b^*$ [see Fig. 3(b)], which lies along the a direction (i.e., the stacks direction). The separation between the two Fermi surface lines is maximum at the border of the Brillouin zone (i.e., the Wigner-Seitz Brillouin zone). Based on this description emerging from

the first-principles calculations, the following remarks can be made.

First, the electronic structure of the anion ordered phase is not obtained by simply perturbing that of the high-temperature structure through the alternating Coulomb potential of the anions; it is a reconstruction built from the band structure of two different stacks with different degrees of dimerization. As shown by the DFT calculations, the Hartree potential of the anions practically does not modify the band dispersion and the largest separation of the Fermi surface sheets is found at the border of the Brillouin zone.

Second, the Fermi surface of the anion ordered structure does not exhibit good nesting properties (see Sec. V A 3). Let us recall that the strongest changes of the Fermi surface upon anion ordering occur at the regions of minimum separation between the two lines (i.e., sheets in a 3D representation). However, these regions are those associated with the k_b wave vectors at the inflexion points of the unperturbed Fermi surface which are those ensuring the good nesting properties. Thus, it seems quite unlikely that the reconstructed Fermi surface can still sustain SDW fluctuations due to nesting in the anion ordered phase exhibiting superconductivity. Consequently, a mechanism based on SDW fluctuations as the driving force for Cooper pair formation, as proposed for $(\text{TMTSF})_2\text{PF}_6$ [80,81], cannot be directly transposed to $(\text{TMTSF})_2\text{ClO}_4$. This suggests that superconductivity in $(\text{TMTSF})_2\text{PF}_6$ under pressure and $(\text{TMTSF})_2\text{ClO}_4$ may be sustained by different mechanisms. Let us note that in the phase diagrams of these salts there is a common border between the superconductivity and SDW regions for pressurized $(\text{TMTSF})_2\text{PF}_6$ [82], whereas superconductivity and SDW are decoupled as a function of the cooling rate in $(\text{TMTSF})_2\text{ClO}_4$ as well as of the ReO_4 content in the $(\text{TMTSF})_2\text{ClO}_{4(1-x)}\text{ReO}_{4x}$ solid solutions [83]. In the latter salts the decoupling is controlled by the microstructure of the anion ordered phase [6,22,84]. In this context it is misleading to place $(\text{TMTSF})_2\text{ClO}_4$ in the generalized phase diagram [82] obtained for salts with octahedral anions such as PF_6 .

Third, in the recent report by Yonezawa *et al.* [76] it has been shown that the nodes or zeros of the superconducting gap in $(\text{TMTSF})_2\text{ClO}_4$ are found in those points of the Fermi surface where the Fermi velocity v_F makes an angle of $\pm 10^\circ$ with the a direction. The points fulfilling this condition using the present first-principles Fermi surface are shown in Fig. 11(a) as orange spots. The $k_b \approx \pm 0.25b^*$ points proposed by Yonezawa *et al.* [76] lending support to d -wave- or g -wave-like superconductivity do not correspond to our orange spots (note also that these authors used a Fermi surface whose inner sheet Fermi velocity does not fulfill their angular condition). Figure 11(a) shows that there are four orange spots which fulfill the $\pm 10^\circ$ angular condition on each Fermi surface sheet: (i) two points that are near the minimum separation of the Fermi surface sheets (Q points) and (ii) two points that are located in the k_b regions of large separation between the Fermi surface sheets. The former set of points, located in the vicinity of Δ_{AO} , are in the region mostly affected by the anion ordering. According to the proposal of nodeless superconductivity by Pratt *et al.* [77], these points could sustain a minimum of the superconducting gap. The latter set of points, present on well-separated Fermi surface sheets, can be linked together to

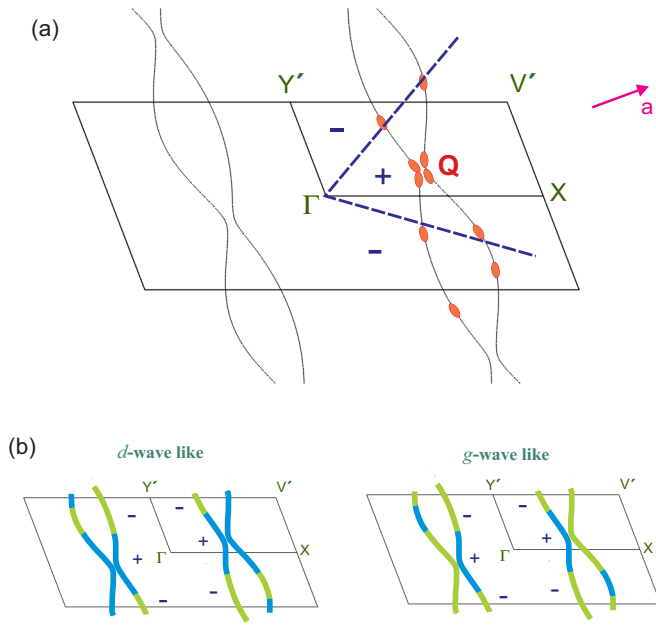


FIG. 11. (Color online) (a) Fermi surface for the anion ordered structure of $(\text{TMTSF})_2\text{ClO}_4$ showing in orange the points of the Fermi surface where the Fermi velocity makes an angle of $\pm 10^\circ$ with the a direction. (b) Schematic representation of plausible d -wave-like and g -wave-like states consistent with the present first-principles calculations of the Fermi surface and the field-angle-resolved calorimetry study by Yonezawa *et al.* [76]. The positive and negative regions of the Fermi surface are represented with different colors.

form two sets of lines going through the Γ point [broken purple lines in Fig. 11(a)]. These lines could correspond to nodes in the superconducting gap as proposed by Yonezawa *et al.* [76]. With an inversion of the sign of the superconducting gap when the lines are crossed when moving parallel to the $\Gamma \rightarrow Y'$ direction on the Fermi surface, this suggests a d -wave-like state [if the sign is the same on the two pairs of sheets of the Fermi surface; see Fig. 11(b)] or a g -wave-like state [if the sign is the opposite on the two pairs of sheets of Fermi surface; see Fig. 11(c)].

Fourth, the shape of the Fermi surface after anion ordering strongly depends on the deformation of the stacks induced by the anion ordering. Of special importance are the elastic deformations originating from the hydrogen bonds established by the ordered anions and the hydrogen atoms of the TMTSF methyl substituents [6]. Consequently, if such deformations are modified, for instance, by quenching or alloying, the shape of the Fermi surface will be affected. In this respect, recent angular magnetoresistance oscillation (AMRO) measurements in the a - c plane [52] provide evidence for substantial modifications of the electronic structure near the Fermi level as a function of the cooling rate. These modifications should particularly affect the minimum of separation between the inner and outer sheets where the magnitude of the anion gap is related to the charge transfer between type A and type B TMTSF molecules (see the Appendix). If we assume that the superconducting gap exhibits a minimum around the Q point, a change of the size of the anion gap upon quenching or alloying may have a noticeable influence on the superconductivity.

Fifth, if the anion ordering is nonhomogeneous, as observed upon quenching or alloying [6,22,84], with coexistence of ordered and nonordered (or badly ordered) domains, the topology of the Fermi surface can exhibit important spatial variations. In this respect, an important aspect of textured $(\text{TMTSF})_2\text{ClO}_4$ is that the electronic interactions should vary spatially because the local order is different around the ordered and nonordered ClO_4 [6]. This is illustrated by the observation of a significant change of lattice parameters with the cooling rate. In particular the c and γ parameters increase (decrease) in the quenched (relaxed) state with respect to their extrapolated high-temperature variation [45,85]. The decrease of c in the relaxed state has to be related to the contraction of the methyl group cavity when the ordered ClO_4 have established its hydrogen bonding network (see Fig. 6). The opening of γ in the relaxed state has to be associated to the shear deformation of the TMTSF layer when TMTSF A, strongly linked to the anion, adopts a boat shape. In addition, high-resolution x-ray measurements [22] show that upon cooling below T_{AO} , the anion ordering process is accompanied by important angular deformations of the lattice consisting mostly on erratic rotations of the c direction, which are probably induced by the formation of local hydrogen bonds together with a concomitant deformation of the linked TMTSFs when an anion orders. All these features show that the anion ordering process, via the progressive setting of its hydrogen bonding network, is accompanied by considerable elastic deformations which should locally modify the electronic interactions. As a consequence, textured $(\text{TMTSF})_2\text{ClO}_4$ should be a superimposition of metallic regions, with a substantially warped and non-nested Fermi surface which achieve a superconducting ground state, and of insulating regions, where the less warped and nested Fermi surface stabilizes a SDW ground state. The previously quoted AMRO data [52] changing drastically as a function of the cooling rate should be analyzed in this framework.

B. Anion ordering in $(\text{TMTSF})_2\text{NO}_3$

$(\text{TMTSF})_2\text{NO}_3$ is a room-temperature metal [29] which at ~ 43 K and ambient pressure exhibits an anion ordering transition [26,27], where, in contrast with $(\text{TMTSF})_2\text{ClO}_4$, the anions order along the direction $(1/2, 0, 0)$, i.e., the direction of maximum conductivity. At the transition, the warped 1D Fermi surface [see Fig. 7(c)] common to all Bechgaard salts becomes a series of compensated electron and hole tubes [see Fig. 8(b)] [25,86], i.e., a 2D Fermi surface, below the anion ordering transition [see Fig. 8(b)]. When further lowering the temperature at ambient pressure, an incommensurate SDW state is stabilized at around 9 K [87]. This SDW state is suppressed by pressure [88–90] (~ 6 –8 kbar) above which the metallic state is kept until very low temperatures without entering into a superconducting state [88,89]. Pressure also shifts the anion ordering transition to higher temperatures (~ 49 K at 7.8 kbar) [90]. Although initial studies showed no sign of magnetic-field-induced spin density wave (FISDW) states [89], their occurrence under pressure was later reported. Vignolles *et al.* [91] showed that they occur at 8.5 kbar above 20 T, presumably arising from the 2D semimetallic state. However, Kang and Chung later reported [90] that at pressures ~ 6.5 –8.5 kbar $(\text{TMTSF})_2\text{NO}_3$ exhibits a Q1D Fermi surface.

These studies suggest that the Fermi surface may experience some reconstruction under such pressures.

How is this behavior related to the electronic structure discussed in Sec. IV? According to the DFT calculations, a nesting vector with transverse component of $0.25b^*$ [see Table I and Fig. 7(c)] is the best nesting vector of the Fermi surface for the average structure at 12 K. This value is in excellent agreement with the experimental value ($\sim 0.25b^*$) reported by Hiraki *et al.* [92] and Satsukawa *et al.* [93]. However, the SDW ordering occurs after the anion-ordering transition so that it is the folded Fermi surface of Fig. 8(b) which must be considered. The average transverse component of the best nesting vector for this Fermi surface is $\sim 0.24b^*$, although this is an imperfect nesting. Namely, the closed hole and electron pockets are best nested for a value of $0.23b^*$ [q_{nest}^h in Fig. 8(b)] and $0.25b^*$ [q_{nest}^e in Fig. 8(b)], respectively. This means that after the SDW ordering, smaller electron and hole pockets will remain so that the system is semimetallic, as experimentally found. However, the fact that the nesting vector of the instability is very similar for the 12 K average and the anion ordered structures suggests that the anion ordering has only a small effect on the Fermi surface. In this respect it is found that the anion ordering gap (Δ_{AO}) is noticeably smaller (8.9 meV) than that of $(\text{TMTSF})_2\text{ClO}_4$. The excellent agreement between the experimental and calculated nesting vectors suggests that, despite creating closed electron and hole orbits, the perturbation of the Fermi surface due to anion ordering is small enough to keep the usual nesting mechanism at the origin of the SDW phase.

In view of this analysis the following question comes immediately into mind: What makes the consequences of the two anion orderings so different? Is it simply related to the different chemical nature of the anion which imposes a different anion ordering gap by forcing stronger/weaker hydrogen bonds between the donor and the anion? We believe that this is not the main reason. Before the occurrence of the anion ordering (i.e., when considering the low-temperature average structure), the best nesting vector is that relating the two inflection points of the warped Fermi surface. Anion ordering folds this Fermi surface so that two sheets connected by the anion ordering wave vector are superposed and cross at some points. The small structural distortion of the donor lattice due to anion ordering makes the mixing of states around the superposition points possible. Thus, when the wave vector of the anion ordering leads to the superposition of the zones around the inflection points, as it happens for the $(0, 1/2, 0)$ ordering of $(\text{TMTSF})_2\text{ClO}_4$, the nesting conditions will be strongly altered. However, when the anion ordering wave vector does not lead to superposition of the zones around the inflection point, as it happens for the $(1/2, 0, 0)$ ordering of $(\text{TMTSF})_2\text{NO}_3$, the perturbation of the nesting conditions will be weak and, despite the existence of closed pockets, a SDW instability at a wave vector very similar to that of the nonanion ordered system will occur. We conclude that the specific wave vector of the anion ordering transition has the main control of the low-temperature instability.

Finally, let us point out that the magnetoresistance study by Kang and Chung [90] suggests that with the restoration of the metallic state above ~ 6.5 – 8.5 kbar, the Fermi surface is open even in the presence of anion ordering. This means that the

$(1/2, 0, 0)$ ordering wave vector cannot survive. In addition, these authors suggest on the basis of the periodicity of Lebed resonances that the b periodicity could be doubled in that pressure range. Given the nature of the Fermi surface before the ordering, the simpler commensurate anion superstructures compatible with an open Fermi surface are those having a zero component along a and a $1/2$ component along b . Thus, both $(0, 1/2, 0)$ and $(0, 1/2, 1/2)$ anion ordered superstructures seem compatible with the previous results. This means that pressurized $(\text{TMTSF})_2\text{NO}_3$ should resemble $(0, 1/2, 0)$ ordered $(\text{TMTSF})_2\text{ClO}_4$ at ambient pressure or $(0, 1/2, 1/2)$ ordered pressurized $(\text{TMTSF})_2\text{ReO}_4$ [94]. In fact, the change from the $(1/2, 0, 0)$ to the $(0, 1/2, 0)$ anion ordering seems not difficult to attain (see Figs. 1 and 9). It can be described as a combination of two types of anion motion. First, a 60° rotation of one every two anions along the a direction brings a uniform anion ordering along a . Second, as shown in Fig. 9, the anion makes short hydrogen bond contacts with two donors at one side of the anion cavity and with one donor on the other side. To change this situation by creating two different types of uniform donor chains as for $(\text{TMTSF})_2\text{ClO}_4$, it would be enough to somewhat shift the anions [most likely along the $(b+c)$ direction] so as to have short contacts with two donors on the same side of the cavity and longer ones on the opposite site. By combining the two motions, a $(0, 1/2, 0)$ anion order is attained. By analogy with $(\text{TMTSF})_2\text{ClO}_4$, one expects that, with this superstructure, the perturbation of the Fermi surface nesting conditions will be stronger and that the stabilization of the SDW order would be less likely than it is in the case of the $(1/2, 0, 0)$ anion ordering. However, the present scenario does not explain why with the same anion order as in $(\text{TMTSF})_2\text{ClO}_4$, superconductivity is not observed in $(\text{TMTSF})_2\text{NO}_3$.

VI. CONCLUDING REMARKS

A first-principles DFT study of the two Bechgaard salts $(\text{TMTSF})_2\text{ClO}_4$ and $(\text{TMTSF})_2\text{NO}_3$ which exhibit anion orderings with two different wave vectors, $(0, 1/2, 0)$ and $(1/2, 0, 0)$, respectively, is reported. It is found that the main effect of the anion ordering on the band structure occurs through the deformations induced in the TMTSF layers (i.e., both the inner structure of the donors and their relative position in the layer) and not through the Coulomb potential of the anions, as it has been almost invariably assumed. The anion ordering in $(\text{TMTSF})_2\text{ClO}_4$ leads to a modulation of the dimerization in successive chains and to a preferred localization of the electronic states around the Fermi level into either the TMTSF A or the TMTSF B chains. The calculated anion ordering gap Δ_{AO} is found to be small but definitely non-nil, ~ 14 meV. The suppression of the SDW instability in the relaxed samples is attributed to the deterioration of nesting in the anion ordered domains. The superconductivity pairing mechanism based on SDW fluctuations achieved by the nesting properties of the single sheet Fermi surface of $(\text{TMTSF})_2\text{PF}_6$ should be reconsidered in $(\text{TMTSF})_2\text{ClO}_4$. Plausible d -wave- and g -wave-like states consistent with the present DFT Fermi surface and a previous field-angle-resolved calorimetry study are proposed. Anion ordering in $(\text{TMTSF})_2\text{NO}_3$ leads to a smaller gap, $\Delta_{AO} = 8.9$ meV. The anion ordering in this phase

leads to a larger charge transfer between the two donors, but to a smaller polarization of the two partially filled bands. The weak influence of anion ordering into the low-temperature physics of this phase is related to the different periodicity of the anion ordering, which leaves the nested parts of the Fermi surface almost unaltered. We conclude that the specific wave vector of the anion ordering together with the deformation induced in the TMTSF stacks have the main control of the low-temperature behavior of these phases. Finally, we propose that it is likely that the anion ordering of $(\text{TMTSF})_2\text{NO}_3$ changes under pressures of 6–8 kbar to become similar to that found for $(\text{TMTSF})_2\text{ClO}_4$.

ACKNOWLEDGMENTS

This work was supported by MINECO-Spain (Grants No. CSD2007-00041, No. FIS2012-37549-C05-05, and No. CTQ2011-23862-C02-02), Generalitat de Catalunya (Grant No. 2009 SGR 1459), and XRQTC. We thank D. Jérôme for useful comments

APPENDIX: SIMPLE MODELS FOR THE ELECTRONIC STRUCTURE OF $(\text{TMTSF})_2\text{ClO}_4$ IN ITS $(0, 1/2, 0)$ ANION ORDERED STATE

With two kinds of TMTSF stacks, A and B, per repeat unit of the superstructure, the electronic structure of the conducting states is given, in its simplest version, by the eigenvalues of the 2×2 tight-binding matrix

$$\begin{pmatrix} \varepsilon_A(k_a) & T_{AB}(k_a, k_b) \\ T_{AB}^*(k_a, k_b) & \varepsilon_B(k_a) \end{pmatrix}. \quad (\text{A1})$$

In principle, with two TMTSF molecules per stack in the repeat unit, $\varepsilon_A(k_a)$, $\varepsilon_B(k_a)$, and $T_{AB}(k_a, k_b)$ should be 2×2 matrices. If we neglect the stack dimerization these 2×2 matrices reduce to simple relations where $\varepsilon_A(k_a)$ and $\varepsilon_B(k_a)$ are the 1D A and B stack dispersions, and where $T_{AB}(k_a, k_b)$ is the interstack coupling. The two conduction band dispersions being the eigenvalues of (A1) are

$$\begin{aligned} \varepsilon_{\pm}(k_a, k_b) &= \{[\varepsilon_A(k_a) + \varepsilon_B(k_a)] \\ &\pm \sqrt{[\varepsilon_A(k_a) - \varepsilon_B(k_a)]^2 + 4|T_{AB}(k_a, k_b)|^2}\}/2. \end{aligned} \quad (\text{A2})$$

In the vicinity of the Fermi level, taken as the origin of energies, the stack dispersions $\varepsilon_A(k_a)$ and $\varepsilon_B(k_a)$ can be linearized,

$$\varepsilon_A(k_a) = \hbar v_F (|k_a| - k_F^A), \quad (\text{A3a})$$

$$\varepsilon_B(k_a) = \hbar v_F (|k_a| - k_F^B). \quad (\text{A3b})$$

Note that for hole dispersions v_F is negative. If one writes $2k_F^0 = k_F^A + k_F^B$ and $2\Delta_{AO} = \hbar v_F (k_F^A - k_F^B)$, Eq. (A2) becomes

$$\varepsilon_{\pm}(k_a, k_b) \approx \hbar v_F (|k_a| - k_F^0) \pm \sqrt{\Delta_{AO}^2 + |T_{AB}(k_a, k_b)|^2}. \quad (\text{A4})$$

The interstack coupling $T_{AB}(k_a, k_b)$ is a blend of interactions along the b , $\sim (b - a/2)$, and $b + a$ directions (see Fig. 10).

Thus, as for the high-temperature dispersion used in Sec. V, this coupling can be written in the form

$$T_{AB}(k_a, k_b) = 2t_b^{AO}(k_a) \cos[k_b b - \Phi^{AO}(k_a)]. \quad (\text{A5})$$

From (A4) the dispersion of the double sheet Fermi surface is obtained by making $\varepsilon_{\pm}(k_a, k_b) = \varepsilon_F = 0$. With $k_a = k_F^0$ in $T_{AB}(k_a, k_b)$ as given by (A5), this dispersion can be simply expressed as

$$k_F^{\pm}(k_b) = k_F^0 \mp \sqrt{\Delta_{AO}^2 + |T_{AB}(k_F^0, k_b)|^2}/(\hbar v_F). \quad (\text{A6})$$

The k_b dependence of the inner $k_F^-(k_b)$ [outer $k_F^+(k_b)$] Fermi surface sheet is respectively due to bonding (antibonding) interactions between the A and B stacks (see discussion in Sec. V A 4). The minimum separation between the two sheets is the anion gap $2\Delta_{AO}$. It occurs for $T_{AB}(k_a, k_b) = 0$. At this k_b there is no AB interstack coupling. The vanishing corresponds also to the inflexion points of the cosine like transverse dispersion (A5). Thus, if intrastack interactions are comparable to those above the anion ordering transition, the anion gap is located in the direction of the best nesting wave vector of the high-temperature Fermi surface. This is basically what the first-principles calculation shows [compare Figs. 2(b) and 3(b)].

The anion gap $2\Delta_{AO}$ involves the difference of the Fermi wave vectors $(k_F^A - k_F^B)$, which amounts to one-quarter of the difference of charge between molecules A and B. Using the first-principles calculation of the charge per molecule A and B of Sec. III, makes it possible to quantitatively account for the value of the minimum of separation of the double sheet Fermi surface of Fig. 3(b).

Expression (A6) obtained for the linearized (A3) intrastack dispersions gives a symmetrical double sheet Fermi surface dispersion. By assuming $t_b^{AO} \gg \Delta_{AO}$, each sheet is warped along k_b by $\sim 2t_b^{AO}$ (in units of $\hbar v_F$).

If one takes into account the next order quadratic term in the development in k_a of $\varepsilon_i(k_a)$ ($i = A$ or B),

$$\frac{\hbar^2 (|k_a| - k_F^i)^2}{2m}, \quad (\text{A7})$$

one obtains an additional contribution in the right member of (A4),

$$\frac{\hbar^2 (|k_a| - k_F^0)^2}{2m} + \frac{\Delta_{AO}^2}{2E_F} \quad (\text{A8})$$

[together with a negligible change of the anion gap Δ_{AO} into $\Delta_{AO}(|k_a|/k_F^0)$ in the square root of (A4)]. In these expressions, m is the hole effective mass and $E_F = m v_F^2/2$ is the Fermi energy. By introducing the value of $(|k_a| - k_F^0)$ calculated from (A6) in Eq. (A8), one obtains a shift of the Fermi surface dispersion with value

$$\left[C + \frac{|T_{AB}(k_F^0, k_b)|^2}{4E_F} \right] / (\hbar v_F). \quad (\text{A9})$$

In (A9) the constant $C \sim \frac{\Delta_{AO}^2}{E_F}$ shifts k_F^0 by a negligible quantity while the $\frac{|T_{AB}(k_F^0, k_b)|^2}{4E_F}$ term contributes to the warping of the Fermi surface. Being of the same sign for the two sheets, the latter contribution introduces a nonsymmetric warping

between the inner and the outer Fermi surfaces which amounts to $(t_b^{AO})^2/E_F$ (in units of $\hbar v_F$) for each sheet. The last quantity, corresponding to the nesting breaking parameter $2t_b'$ used in the literature and in Sec. V A 3, leads to an asymmetry ratio,

$$\frac{t_b'}{t_b^{AO}} \approx \frac{t_b}{2E_F} \sim 0.15, \quad (\text{A10})$$

by taking $t_b = 50$ meV from Table I and $E_F = 170$ meV from Fig. 3(a). The measurement of the relative warping of the inner and outer first-principles Fermi surfaces shown in Fig. 3(b) gives a similar ratio of 0.20.

The dispersion used in the literature to describe the effect of the anion ordering on the electronic structure is obtained by folding the high-temperature dispersion $\varepsilon(k_a, k_b)$ as a consequence of the superstructure anion potential $V(y) = V \cos(Q_y)$, where $Q = b^*/2$. More quantitatively this dispersion corresponds to the eigenvalues of the 2×2 matrix

$$\begin{pmatrix} \varepsilon(k_a, k_b) & V \\ V & \varepsilon(k_a, k_b + Q) \end{pmatrix}, \quad (\text{A11})$$

which are

$$\varepsilon'_{\pm}(k_a, k_b) = \{[\varepsilon(k_a, k_b) + \varepsilon(k_a, k_b + Q)] \pm \sqrt{[\varepsilon(k_a, k_b) - \varepsilon(k_a, k_b + Q)]^2 + 4V^2}\}/2. \quad (\text{A12})$$

For a linearized dispersion in the stack direction and using the effective transverse dispersion given at the beginning of Sec. V, one obtains

$$\varepsilon'_{\pm}(k_a, k_b) \approx \hbar v_F (|k_a| - k_F^0) \pm \sqrt{V^2 + 4t_b^2 \cos^2(k_b b - \Phi)}. \quad (\text{A13})$$

As before, $\varepsilon'_{\pm}(k_a, k_b) = \varepsilon_F = 0$ leads to a double sheet Fermi surface,

$$k_F^{\pm}(k_b) = k_F^0 \mp \sqrt{V^2 + 4t_b^2 \cos^2(k_b b - \Phi)}/(\hbar v_F). \quad (\text{A14})$$

Equation (A14) exhibits the same type of dispersion as (A6). The minimum of separation between the two sheets, the anion gap $2V$, occurs also for the k_b at which the cosine vanishes. It is located on the inflexion points of the high-temperature Fermi surface. Basically, the same minimum condition obtained with (A6) is recovered. However, in (A14) V is related to the anion Hartree potential, whereas in (A6) Δ_{AO} is related to the charge transfer between the A and B stacks so that they correspond to different microscopic quantities. The first-principles calculations reported in the main text show that V contributes only around one-third of the value of the anion gap.

-
- [1] D. Jérôme, A. Mazaud, M. Ribault, and K. Bechgaard, *J. Phys. Lett.* **41**, L95 (1980).
- [2] D. Jérôme and H. J. Schulz, *Adv. Phys.* **31**, 299 (1982).
- [3] T. Ishiguro, K. Yamaji, and G. Saito, *Organic Superconductors*, 2nd ed. (Springer-Verlag, Heidelberg, 1998).
- [4] G. Rindorf, H. Soling, and N. Thorup, *Acta Crystallogr., Sect. B: Struct. Crystallogr. Cryst. Chem.* **38**, 2805 (1982).
- [5] P. M. Grant, *J. Phys. (Paris)* **44**, C3-847 (1983).
- [6] J.-P. Pouget, *Crystals* **2**, 466 (2012).
- [7] J. P. Pouget and S. Ravy, *J. Phys. I* **6**, 1501 (1996).
- [8] S. Ishibashi, A. A. Manuel, and M. Kohyama, *J. Phys.: Condens. Matter* **11**, 2279 (1999).
- [9] S. Ishibashi and M. Kohyama, *Phys. Rev. B* **62**, 7839 (2000).
- [10] C. Rovira, J. J. Novoa, J. L. Mozos, P. Ordejón, and E. Canadell, *Phys. Rev. B* **65**, 081104 (2002).
- [11] Y. J. Lee, R. M. Nieminen, P. Ordejón, and E. Canadell, *Phys. Rev. B* **67**, 180505(R) (2003).
- [12] J. Fraxedas, Y. J. Lee, I. Jiménez, R. Gago, R. M. Nieminen, P. Ordejón, and E. Canadell, *Phys. Rev. B* **68**, 195115 (2003).
- [13] S. Ishibashi, K. Terakura, and A. Kobayashi, *J. Phys. Soc. Jpn.* **77**, 24702 (2008).
- [14] N. Tenn, N. Bellec, O. Jeannin, L. Piekara-Sady, P. Auban-Senzier, J. Íñiguez, E. Canadell, and D. Lorcy, *J. Am. Chem. Soc.* **131**, 16961 (2009).
- [15] P. Foury-Leylekian, J.-P. Pouget, Y.-J. Lee, R. M. Nieminen, P. Ordejón, and E. Canadell, *Phys. Rev. B* **82**, 134116 (2010).
- [16] P. Alemany, J.-P. Pouget, and E. Canadell, *Phys. Rev. B* **85**, 195118 (2012).
- [17] A. C. Jacko, H. Feldner, E. Rose, F. Lissner, M. Dressel, R. Valentí, and H. O. Jeschke, *Phys. Rev. B* **87**, 155139 (2013).
- [18] J.-P. Pouget, P. Foury-Leylekian, P. Alemany, and E. Canadell, *Phys. Stat. Solidi B* **249**, 937 (2012).
- [19] K. Bechgaard, K. Carneiro, M. Olsen, F. B. Rasmussen, and C. S. Jacobsen, *Phys. Rev. Lett.* **46**, 852 (1981).
- [20] J. P. Pouget, G. Shirane, K. Bechgaard, and J. M. Fabre, *Phys. Rev. B* **27**, 5203 (1983).
- [21] D. Le Pévelin, J. Gaultier, Y. Barrans, D. Chasseau, F. Castet, and L. Ducasse, *Eur. Phys. J. B* **19**, 363 (2001).
- [22] J. P. Pouget, S. Kagoshima, T. Tamegai, Y. Nogami, K. Kubo, T. Nakajima, and K. Bechgaard, *J. Phys. Soc. Jpn.* **59**, 2036 (1990).
- [23] Y. Nagai, H. Nakamura, and M. Machida, *Phys. Rev. B* **83**, 104523 (2011).
- [24] V. J. Emery, *J. Phys. (Paris)* **44**, C3-977 (1983).
- [25] P. M. Grant, *Phys. Rev. Lett.* **50**, 1005 (1983).
- [26] J. P. Pouget, R. Moret, R. Comès and K. Bechgaard, *J. Phys. Lett. (Paris)* **42**, L543 (1981).
- [27] Y. Barrans, J. Gaultier, S. Bracchetti, P. Guionneau, D. Chasseau, and J. M. Fabre, *Synth. Met.* **103**, 2042 (1999).
- [28] A. Mazaud, Ph.D. thesis, Université Paris-Sud, 1981.
- [29] K. Bechgaard, C. S. Jacobsen, H. J. Pedersen, and N. Thorup, *Solid State Commun.* **33**, 1119 (1980).
- [30] P. Hohenberg and W. Kohn, *Phys. Rev.* **136**, B864 (1964).
- [31] W. Kohn and L. J. Sham, *Phys. Rev.* **140**, A1133 (1965).
- [32] J. M. Soler, E. Artacho, J. Gale, A. García, J. Junquera, P. Ordejón, and D. Sánchez-Portal, *J. Phys.: Condens. Matter* **14**, 2745 (2002).
- [33] E. Artacho, E. Anglada, O. Dieguez, J. D. Gale, A. García, J. Junquera, R. M. Martin, P. Ordejón, J. M. Pruneda, D. Sánchez-Portal, and J. M. Soler, *J. Phys.: Condens. Matter* **20**, 064208 (2008).

- [34] For more information on the SIESTA code, visit <http://www.icmab.es/siesta/>
- [35] For a review on applications of the SIESTA approach in materials science, see D. Sánchez-Portal, P. Ordejón, and E. Canadell, *Struct. Bonding (Berlin)* **113**, 103, 2004.
- [36] J. P. Perdew, K. Burke, and M. Ernzerhof, *Phys. Rev. Lett.* **77**, 3865 (1996).
- [37] N. Troullier and J. L. Martins, *Phys. Rev. B* **43**, 1993 (1991).
- [38] L. Kleinman and D. M. Bylander, *Phys. Rev. Lett.* **48**, 1425 (1982).
- [39] E. Artacho, D. Sánchez-Portal, P. Ordejón, A. García, and J. M. Soler, *Phys. Status Solidi B* **215**, 809 (1999).
- [40] H. J. Monkhorst and J. D. Pack, *Phys. Rev. B* **13**, 5188 (1976).
- [41] B. Gallois, Ph.D. thesis, Université de Bordeaux I, 1987.
- [42] D. Le Pévelin, Ph.D. thesis, Université de Bordeaux I, 1999.
- [43] S. Hebrard-Bracchetti, Ph.D. thesis, Université de Bordeaux I, 1996.
- [44] L. Ducasse, M. Abderrabba, J. Hoarau, M. Pesquer, B. Gallois, and J. Gaultier, *J. Phys. C.: Solid State Phys.* **19**, 3805 (1986).
- [45] P. Fertey, E. Canadell, J. P. Pouget, F. Sayetat, C. Lenoir, P. Batail, and J. Muller, *Synth. Met.* **70**, 761 (1995).
- [46] P. Auban-Senzier, D. Jérôme, N. Doiron-Leyraud, S. René de Cotret, A. Sedeki, C. Bourbonnais, L. Taillefer, P. Alemany, E. Canadell, and K. Bechgaard, *J. Phys.: Condens. Matt.* **23**, 345702 (2011).
- [47] K. Yamaji, *J. Phys. Soc. Jpn.* **51**, 2787 (1982).
- [48] $t_a = (t_{s1} + t_{s2})/2$; $t_b^+ = (t_{l3} + t_{l4})$; $t_b^- = (t_{l1} + t_{l2})/2$; $t_b = \{[(t_b^-)^2 + (\sqrt{2}t_b^+ + t_b^-)^2]/\sqrt{2}\}^{1/2}$; $\tan \Phi = t_b^- / (\sqrt{2}t_b^+ + t_b^-)$.
- [49] W. Henderson, V. Vescoli, P. Tran, L. Degiorgi, and G. Grüner, *Eur. Phys. J. B* **11**, 365 (1999).
- [50] F. Guo, K. Murata, H. Yoshino, S. Maki, S. Tanaka, J. Yamada, S. Nakatsuji, and H. Anzai, *J. Phys. Soc. Jpn.* **67**, 3000 (1998).
- [51] H. Schwenk, K. Andres, and F. Wudl, *Phys. Rev. B* **29**, 500 (1984).
- [52] Ya A. Gerasimenko, V. A. Prudkoglyad, A. V. Kornilov, S. V. Sanduleanu, J. S. Qualls, and V. M. Pudalov, *JETP Lett.* **97**, 419 (2013).
- [53] J. M. Delrieu, M. Roger, C. Coulon, R. Laversanne, and E. Dupart, *Synth. Met.* **27**, B35 (1988).
- [54] M. Roger, J. M. Delrieu, and E. W. Mboague, *Phys. Rev. B* **34**, 4952 (1986).
- [55] L. Ducasse, M. Abderrabba, and B. Gallois, *J. Phys. C: Solid State Phys.* **18**, L-947 (1985).
- [56] X. Yan, M. J. Naughton, R. V. Chamberlin, L. Y. Chiang, S. Y. Hsu, and P. Chaikin, *Synth. Met.* **27**, B145 (1988).
- [57] S. Haddad, S. Charfi-Kaddour, M. Héritier, and R. Bennaceur, *Phys. Rev. B* **72**, 085104 (2005).
- [58] S. Haddad, M. Heritier, and S. Cherfi-Kaddour in *The Physics of Organic Superconductors and Conductors*, edited by A. Lebed (Springer, Heidelberg, 2008), p. 605.
- [59] S. Uji, T. Terashima, H. Aoki, J. S. Brooks, M. Tokumoto, S. Takasaki, J. Yamada, and H. Anzai, *Phys. Rev. B* **53**, 14399 (1996).
- [60] H. Yoshino, A. Oda, T. Sasaki, T. Hanajiri, J. Yamada, S. Nakatsuji, H. Anzai, and K. Murata, *J. Phys. Soc. Jpn.* **68**, 3142 (1999).
- [61] H. Yoshino, S. Shodai, and K. Murata, *Synth. Met.* **133-134**, 55 (2003).
- [62] A. G. Lebed, H. I. Ha, and M. J. Naughton, *Phys. Rev. B* **71**, 132504 (2005).
- [63] H. I. Ha, A. G. Lebed, and M. J. Naughton, *Phys. Rev. B* **73**, 033107 (2006).
- [64] H. Yoshino and K. Murata in *The Physics of Organic Superconductors and Conductors*, edited by A. Lebed (Springer, Heidelberg, 2008), p. 433.
- [65] K. Sengupta and N. Dupuis, *Phys. Rev. B* **65**, 035108 (2001).
- [66] D. Zanchi and A. Bjelis, *Europhys. Lett.* **56**, 596 (2001).
- [67] Y. Hasegawa and K. Kishigi, *Phys. Rev. B* **78**, 045117 (2008).
- [68] X. Huang and K. Maki, *Phys. Rev. B* **46**, 162 (1992).
- [69] V. Vescoli, L. Degiorgi, M. Dressel, A. Schwartz, W. Henderson, B. Alavi, G. Grüner, J. Brinckmann, and A. Virosztek, *Phys. Rev. B* **60**, 8019 (1999).
- [70] M. Ribault, *Mol. Cryst. Liq. Cryst.* **119**, 91 (1985).
- [71] N. Matsunaga, K. Hino, T. Ohta, K. Yamashita, K. Nomura, T. Sasaki, A. Ayari, P. Monceau, M. Watanabe, J. Yamada, and S. Nakatsuji, *J. Phys. IV (France)* **131**, 269 (2005).
- [72] H. Kowada, R. Kondo, and S. Kagoshima, *J. Phys. Soc. Jpn.* **76**, 114710 (2007).
- [73] H. Shimahara, *Phys. Rev. B* **61**, R14936 (2000).
- [74] Y. Mizuno, A. Kobayashi, and Y. Suzumura, *Physica C* **471**, 49 (2011).
- [75] B. J. Powell, *J. Phys.: Condens. Matter* **20**, 345234 (2008).
- [76] S. Yonezawa, Y. Maeno, K. Bechgaard, and D. Jérôme, *Phys. Rev. B* **85**, 140502(R) (2012).
- [77] F. L. Pratt, T. Lancaster, S. J. Blundell, and C. Baines, *Phys. Rev. Lett.* **110**, 107005 (2013).
- [78] J. P. Pouget, C. Noguera, A. H. Moudden, and R. Moret, *J. Phys. (Paris)* **46**, 1731 (1985).
- [79] E. Canadell and M.-H. Whangbo, *Chem. Rev.* **91**, 965 (1991) (see sections 10.2 and 9.3).
- [80] C. Bourbonnais and A. Sedeki, *Phys. Rev. B* **80**, 085105 (2009).
- [81] A. Sedeki, D. Bergeron, and C. Bourbonnais, *Phys. Rev. B* **85**, 165129 (2012).
- [82] D. Jérôme, *Science* **252**, 1509 (1991).
- [83] N. Joo, P. Auban-Senzier, C. R. Pasquier, D. Jérôme, and K. Bechgaard, *Europhys. Lett.* **72**, 645 (2005).
- [84] V. Ilakovac, S. Ravy, K. Boubekeur, C. Lenoir, P. Batail, and J. P. Pouget, *Phys. Rev. B* **56**, 13878 (1997).
- [85] P. Fertey, F. Sayetat, J. Muller, J. P. Pouget, C. Lenoir, and P. Batail, *Physica C* **235-240**, 2459 (1994).
- [86] W. Kang, K. Behnia, D. Jérôme, L. Balicas, E. Canadell, M. Ribault, and J. M. Fabre, *Europhys. Lett.* **29**, 635 (1995).
- [87] L. P. Le, A. Keren, G. M. Luke, B. J. Sternlieb, W. D. Wu, Y. J. Uemura, J. H. Brewer, T. M. Riseman, R. V. Upasani, L. Y. Chiang, W. Kang, P. M. Chaikin, T. Csiba, and G. Gruner, *Phys. Rev. B* **48**, 7284 (1993).
- [88] D. Jérôme, *Mol. Cryst. Liq. Cryst.* **79**, 511 (1982).
- [89] W. Kang, S. T. Hannahs, L. Y. Chiang, R. Upasani, and P. M. Chaikin, *Phys. Rev. Lett.* **65**, 2812 (1990).
- [90] W. Kang and O.-H. Chung, *Phys. Rev. B* **79**, 045115 (2009).
- [91] D. Vignolles, A. Audouard, M. Nardone, L. Brossard, S. Bouguessa, and J.-M. Fabre, *Phys. Rev. B* **71**, 020404(R) (2005).
- [92] K. Hiraki, T. Nemoto, T. Takahashi, H. Kang, Y. Jo, W. Kang, and O.-H. Chung, *Synth. Met.* **135-136**, 691 (2003).
- [93] H. Satsukawa, K. Hiraki, T. Takahashi, H. Kang, Y. J. Jo, and W. Kang, *J. Phys IV (France)* **114**, 133 (2004).
- [94] R. Moret, S. Ravy, J. P. Pouget, R. Comès, and K. Bechgaard, *Phys. Rev. Lett.* **57**, 1915 (1986).